FRICTION STIR WELDING PROCESS PARAMETER OPTIMIZATION OF AL6061-T6 ALLOYS

by

Denizhan Akbal

A Dissertation Submitted to the

Graduate School of Sciences and Engineering

in Partial Fulfillment of the Requirements for

the Degree of

Master of Science

in

Mechanical Engineering

KOÇ ÜNİVERSİTESİ

December 2022

FRICTION STIR WELDING PROCESS PARAMETER OPTIMIZATION OF AL6061-T6 ALLOYS

Koç University

Graduate School of Sciences and Engineering

This is to certify that I have examined this copy of a master's thesis by

Denizhan Akbal

and have found that it is complete and satisfactory in all respects,

and that any and all revisions required by the final

examining committee have been made.

Committee Members:

____

Assoc. Prof. Arif Karabeyoğlu [Advisor]

____

Assist. Prof. Kaan Bilge [Co-Advisor]

____

Prof. Demircan Canadinç

____

Prof. İbrahim Özkol

Date: ______________________________

This thesis is dedicated to my precious family, my darling wife, and my dear friends, who have supported me throughout this journey, my co-advisor Assist. Prof. Kaan Bilge for his endless support and valuable contributions, as well as my thesis advisor Assoc. Prof. Arif Karabeyoğlu, who has been a beacon of wisdom and motivation for me with his mastership.

ABSTRACT

In this study, Al6061-T6 plates are welded together with ‘Friction Stir Welding’ (FSW) method. Experimentations are performed within a design of experiments scheme. A full factorial design with three parameters such as; welding speed, rotational speed, and downward force at three levels (maximum, mean, minimum) with 27 design points is employed.

Half of the manufactured plates are then subjected to artificial ageing process resulting as a total of 54 different experiment points. Manufactured plates are cut into tensile specimens according to ASTM E8 standards. Tensile tests are performed in order to find out three mechanical properties: Yield Stress, Ultimate Tensile Stress, and Strain at UTS. Un-aged yield stress, un-aged UTS, aged yield stress, and aged UTS values were employed as responses to polynomial surrogate models taking process parameters (welding speed, rotational speed, downward force) as variables. Response surface methodology is then used to estimate the model constants associated with the singular or combinative effects of process parameters on measured responses. Model qualities for each response is measured by ANOVA analysis and are reported. With a very high level of confidence surrogate models with R^2= 0.92 was obtained for aged UTS values.

Metallographic analysis is also performed to visualize selected experimentation points to determine the shape of formed weld zones namely, weld nugget zone (WNZ), thermos-mechanically affected zone (TMAZ), and heat affected zone (HAZ) as well as the amount of base material prior to the processing in corresponding zones.

ÖZETÇE

Bu çalışmada Al6061-T6 plakalarının ‘Sürtünme Karıştırma Kaynağı’ metodu ile kalıcı birleştirilmesi yapılmıştır. Yapılan deney planı için tam faktöriyel tasarım kullanılmıştır ve parametre olarak; ilerleme hızı, dönme hızı, ve baskı kuvveti seçilmiştir. Bu parametreler üç seviyede (maksimum, orta, minimum) incelenerek toplam 27 deney noktası elde edilmiştir.

Üretilen numunelerin yarısı yapay yaşlandırma yönteminden geçirilmiş, toplamda 54 farklı veri noktası elde edilmiştir. Kaynatılan plakalar mekanik çekme testinden geçirilmek üzere ASTM E8 standardında kesilmiştir. Mekanik çekme testleri malzemelerin; akma direnci, kopma direnci ve kopma uzaması değerlerini bulmak için yapılmıştır. Belirlenen parametreler bağımsız değişken, yaşlandırılmamış akma ve kopma direnci, ve yaşlandırılmış akma ve kopma direnci sonuç olacak şekilde matematiksel modeller oluşturulmuştur. Tepki yüzey analizi yöntemiyle modeldeki tekil veya birleşik parametrelerin katsayıları belirlenmiştir. Her bir sonuç için model kaliteleri ANOVA analizi ile ölçülmüş ve raporlanmıştır. Yaşlanmış kopma direnci modelinde R^2= 0.92 gibi çok yüksek bir değer elde edilmiştir.

Numunelerin aynı zamanda kaynak bölgelerindeki mikroyapıyı incelemek ve farklı kaynak bölgelerinin (Kaynak Merkezi, Termo-mekanik Etki Altındaki Bölge, Isı Tesiri Altındaki Bölge) tespitini yapabilmek için kesit bölgelerinden metalografi incelemeleri yapılmıştır.

ACKNOWLEDGEMENTS

For helping me complete this study, I would like to thank to my advisor Arif Karabeyoğlu and my co-advisor Kaan Bilge for trusting in me and guiding me throughout this journey. I also thank to DeltaV Uzay Teknolojileri A.Ş. and its staff for providing me the necessary tools and resources to complete this project. I also wish to extend my special thanks to Kadir Çıtak from CKF Technology and Consulting for providing technical consultancy and help with the FSW operations.

TABLE OF CONTENTS

LIST OF TABLES viii

LIST OF FIGURES ix

ABBREVIATIONS xi

CHAPTERA1: INTRODUCTION 1

CHAPTER 2: LITERATURE REVIEW 7

CHAPTER 3: FSW PROCESS DYNAMICS 10

CHAPTER 4: METHODOLOGY 15

4.1 Plate Preparation 15

4.2 Tool-Fixture Design and FSW Machine 16

4.3 Experimental Design and Welding Parameters 18

4.4 Post-Processing of Plates 19

4.5 Response Surface Methodology 23

4.5.1 Full-Factorial Design 23

4.5.2 Determination of Parameter Ranges 24

4.5.3 Responses 25

Regression Analysis 26

4.6 Microscopy 26

CHAPTER 5: RESULTS AND DISCUSSION 29

5.1 Data Evaluation and Grouping 29

5.2 Effect of Process Parameters with Analysis of Variance Method 36

5.3 Optimization 53

5.4 Model Verification Tests 55

CHAPTER 6: CONCLUSION 56

6.1 Final Remarks 56

6.2 Future Works 56

BIBLIOGRAPHY 57

LIST OF TABLES

Table 4. 1: Variable Values of Welding Parameters. 19
Table 4. 2: Constant Welding Parameters of the Process 19
Table 4. 3: Full Factorial Design and Hardness Values. 20
Table 4. 4: Full Factorial Design of Experiments. 24
Table 4. 5: Range of Parameters. 25

Table 5. 1: Mechanical Properties of Base Material-26, Un-Aged FSW-26 and Aged FSW-26. 30
Table 5. 2: Overall Results for Un-Aged and Aged Al6061-T6 Samples. 35
Table 5. 3: Fit Summary for Un-Aged UTS. 37
Table 5. 4: ANOVA for Linear Model Response: UTS. 37
Table 5. 5: Final Equation in Terms of Coded Factors. 37
Table 5. 6: Fit Summary for Un-Aged Yield Stress. 40
Table 5. 7: ANOVA for Quadratic Model Response: Un-Aged Yield Stress. 40
Table 5. 8: Final Equation in Terms of Coded Factors. 41
Table 5. 9: Fit Summary for Aged Yield Stress. 44
Table 5. 10: ANOVA for Quadratic Model Response: Aged-Yield Stress. 45
Table 5. 11: Final Equation in Terms of Coded Factors. 45
Table 5. 12: Fit Summary for Aged Yield Stress. 49
Table 5. 13: ANOVA for Quadratic Model Response: Aged-UTS. 49
Table 5. 14: Final Equation in Terms of Coded Factors. 50
Table 5. 15: Final Equations of All Responses in Terms of Coded Factors. 53
Table 5. 16: Model Verification Test Results. 55

LIST OF FIGURES

Figure 1.1: General Schematic of FSW Process in Butt Welding Configuration [Mishra et. al., 2014]. 2
Figure 1.2: FSW Process Microstructural Zones [Mishra et. al., 2014]. 3
Figure 1.3: Advantages of Friction Stir Welding [Mishra et. al., 2014]. 5

Figure 2. 1: Triflute Tool Prototype [Kallee et. al., 2001]. 8
Figure 2. 2: J. Boonma et. al. Hardness values of as welded and PWHT Samples [Boonma et. al., 2015]. 9

Figure 3. 1: General Shape of a Tool with Conical Shoulder Surface [Mishra et. al., 2014]. 11
Figure 3. 2: Infinitesimal Elements of Different Frictional Heating Contributors on the Tool [Mishra et. al., 2014]. 12

Figure 4. 1: Metal Spectrometer. 15
Figure 4. 2: Flaw Mechanisms: (a) Root Flaw, (b) Toe Flash. 16
Figure 4. 3: Plate Dimensions. 16
Figure 4. 4: FSW Tool. 17
Figure 4. 5: FSW Fixture. 17
Figure 4. 6: FSW Fixture Design for CNC Machine. 17
Figure 4. 7: FSW Machine. 18
Figure 4. 8: Tilt Angle Setup and FSW Process. 18
Figure 4. 9: Hardness Measurements. 20
Figure 4. 10: Radiographic Image of FSW-07 Plate. 21
Figure 4. 11: Sample Layout. 22
Figure 4. 12: Tensile Tests. 23
Figure 4. 13: FSW-13-07 Stress Strain Curve 26
Figure 4. 14: Different Fracture Zone Types... 27
Figure 4. 15: Top Views of Fracture Surfaces. 28
Figure 4. 16: Side Views of Fracture Surfaces 28

Figure 5. 1: (a) Base Materal-26, (b) Un-Aged FSW-26 and (c) Aged FSW-26. 30
Figure 5. 2: Different Microstructural Zones and Interfaces. 30
Figure 5. 3: Metallography Images of Un-Aged FSW-26 Specimens. 31
Figure 5. 4: Stereo Microscope Image of the Weld Zone for FSW-26 Un-Aged and Aged (respectively). 31
Figure 5. 5: Un-Aged Tensile Test Specimens Strain vs. UTS. 32
Figure 5. 6: Aged and Un-Aged Specimens - UTS vs. Strain Graph. 33
Figure 5. 7: Aged and Un-Aged Specimens - UTS vs. YS Graph. 33
Figure 5. 8: Predicted vs. Actual Values: Un-Aged UTS. 38
Figure 5. 9: Radiography Images of Samples 7-8-9 (respectively from top to bottom)...... 38
Figure 5. 10: Cube Plot of Data Points for Un-Aged UTS. 39
Figure 5. 11: Predicted vs. Actual Values: Un-Aged Yield Stress. 42
Figure 5. 12: Stereo Microscope Images of Un-Aged Metallography Samples from (a) No. 24, (b) No. 26 Weld Plates 43
Figure 5. 13: 3D Surface Plot of the Model of Rotational Speed vs. Welding Speed vs. Yield Stress ((a)Down Force = -1, (b)Down Force = 0, (c) Down Force = 1). 43
Figure 5. 14: Cube Plot of Data Points for Un-Aged Yield Stress. 44
Figure 5. 15: Predicted vs. Actual Values: Aged Yield Stress. 46
Figure 5. 16: Stereo Microscope Images of Aged Metallography Samples from (a) No. 24 and (b) No. 26 Weld Plates. 47
Figure 5. 17: 3D Surface Plot of the Model of Rotational Speed vs. Welding Speed vs. Aged-Yield Stress ((a) Down Force = -1, (b) Down Force = 0 and (c) Down Force = 1). 47
Figure 5. 18: Cube Plot of Data Points for Aged Yield Stress. 48
Figure 5. 19: Predicted vs. Actual Values: Aged UTS. 50
Figure 5. 20: 3D Surface Plot of the Model of Rotational Speed vs. Welding Speed vs. Aged-UTS ((a) Down Force = -1, (b) Down Force = 0 and (c) Down Force = 1). 51
Figure 5. 21: Cube Plot of Data Points for Aged UTS. 52
Figure 5. 22: Criteria for Optimization. 53
Figure 5. 23: Solution Values. 54
Figure 5. 24: Solution Contour Graph. 54

ABBREVIATIONS

FSW	Friction Stir Welding
YS	Yield Stress
UTS	Ultimate Tensile Stress
ANOVA	Analysis of Variance
WNZ	Weld Nugget Zone
TMAZ	Thermo-Mechanically Affected Zone
HAZ	Heat Affected Zone
RS	Rotational Speed
WS	Welding Speed
DF	Down Force

CHAPTER 1:
INTRODUCTION

Joining of materials is a crucial concept in design, manufacturing, and engineering in general. Competence at joining, enable the design process to become more sophisticated by allowing one to work with advanced materials and complex geometries. It is also vital in manufacturing large integrated systems as these joints literally hold structures together. Joining of materials is achieved via two main processes: mechanical connections or metallurgical bonding.

Metallurgical bonding processes of metals can be divided into four categories: fusion welding, brazing and soldering, adhesive bonding, and solid-state bonding. Fusion welding is the most common technique utilized in industrial applications. During fusion welding, either the base materials or a filler material in between the joint line is melted via heat created by an electrical arc and desired pieces of metal are joined together as the liquified zone quickly solidifies when the heat source is removed. In brazing and soldering process, only the filler material is melted, and the molten metal solidifies in the space between the two base metals to be joined. As the filler solidifies, it creates the bond between the two metals. Adhesive bonding is similar to soldering and brazing, but the filler material used in this process is some type of glue rather than molten metal. Finally, solid-state bonding process is the hardest technique as it utilizes both the plastic deformation and atomic diffusion mechanisms to create new atomic bonds between two separate base metals thus resulting in joining them [Mishra et. al., 2014]. In this process no foreign material is used as well as no melting/solidification occurs as both these properties among many others make solid-state bonding supreme among all metal bonding processes.

Friction stir welding (FSW) is a solid-state bonding technique that was invented in 1991 by Wayne Thomas at The Welding Institute (TWI). Ever since the introduction of FSW, it quickly found itself a place in a variety of sectors such as aerospace, automobile, electronics etc. [ISO, 2020]. Further advancement of FSW technology enables it to be utilized in different areas of industry, replacing fusion welding as post-weld properties of FSW are superior to those of fusion.

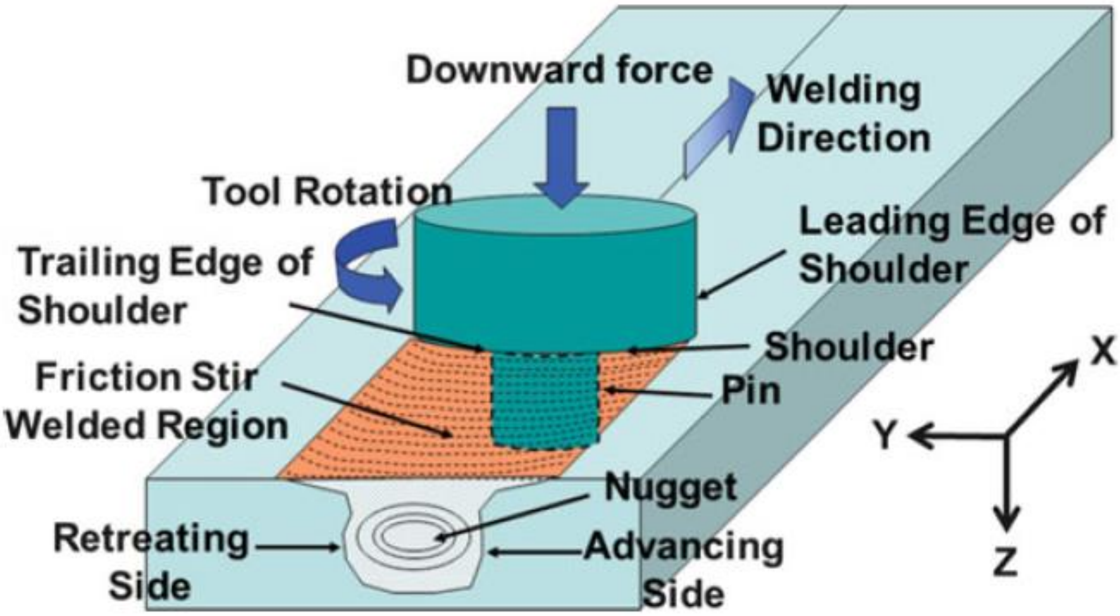

Figure 1.1: General Schematic of FSW Process in Butt Welding Configuration [Mishra et. al., 2014].

There are many different types of FSW process configurations, differing in the type of tool that is used or the placement of plates to be welded. For the scope of this thesis, the FSW process of Al6061 alloys with non-consumable rotating tools in butt welding configuration will be investigated, as it can be seen in Fig. 1.1.

During FSW process, solid-state bonding is achieved by plastic deformation and diffusion bonding [Lee et. al., 2020]. The tool seen in Fig. 1.1 creates the heat and pressure, required for the atoms to diffuse among the joint line and to form new atomic bonds as they are mixed and pressed into each other. Originally there are two separate base plates abutted to each other where the joint line passes in between. The FSW tool rotates and presses down this joint line to create frictional heating, pressure, and mixing. Heat is utilized to bring the welding zone to high temperatures below the melting point of base metals. At elevated temperatures these metals get plasticized and, deformation and diffusion occur with more ease. During this plasticized state, tool pin that is submerged in the welding region rotates and flows the material from one side to the other, mixing the material. Meanwhile, pressure is applied by the tool shoulder in vertical direction. By this applied pressure, flowing material is contained underneath the tool and atoms are forced into close contact with each other as atomic attraction creates new bonds [Mishra et. al., 2014].

FSW tool creates heat both by frictional heating and adiabatic dissipative heating during plastic deformation. As tool approaches, frictional heat conducting through the region at the front and as it passes by, both frictional and deformational heating elevates the temperature of the weld zone to a near melting point, although not reaching it thus not liquifying the metal. After this encounter the tool traverses further along the joint line and the weld zone quickly cools and sort of solidifies. When the tool passes through it quickly mixes and deforms the material at high temperatures. Due to this strong plastic deformation at below-near melting points, microstructural changes happen, especially in the nugget zone as fully recrystallized, equiaxed, fine grain microstructure is observed in this region. This main output in the nugget zone is crucial as it results in outstanding mechanical and fatigue properties.

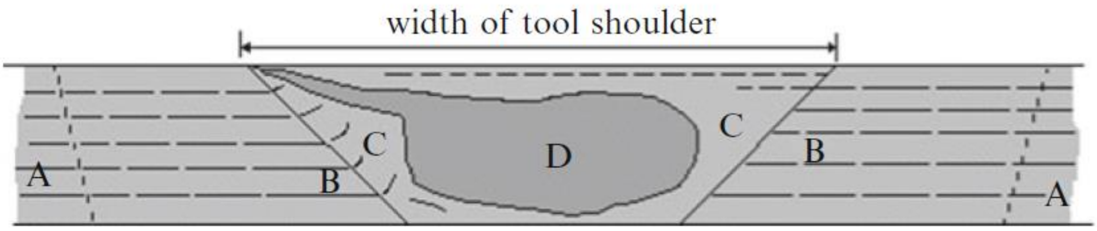

Figure 1.2: FSW Process Microstructural Zones [Mishra et. al., 2014].

There are four main microstructural zones in the stir-welded cross-sectional view, as it can be seen from Fig. 1.2. Region 'A' is the base metal that is not influenced by either mechanical deformations nor heating effects. Region 'B' is the heat affected zone (HAZ), where mainly the frictional heat created by the shoulder of the tool causes some microstructural changes as it experiences a thermal cycle. This region does not plastically deform and is observed in fusion welding as well. Region 'C' is thermo-mechanically affected zone (TMAZ), where microstructural changes happen both because of plastic deformation and heat. Material in this region is subjected to plastic deformation strain and recrystallization is mostly not present. Region 'D' is the weld nugget, also called the stir zone. This region has a distinct macroscopic feature as 'onion rings' shaped distributions can be observed in the cross section. Weld nugget has recrystallized, fine grain microstructure because of immense plastic deformation and elevated temperature. This zone is more affected by the pin that is submerged in the base metal during FSW, compared to the other regions. Weld nugget is very crucial in the sense of quality of the weld, since voids, cracks and insufficient mechanical behavior is usually observed in this region, thus failures of the weld stemming out of it [ISO, 2020]. Shape and dimensions of the tool pin is very significant affecting the possible failure mechanisms in the stir zone.

Friction stir welding process has many parameters that factor in the production and affecting the outcome of the weld. These parameters are important to fully understand this fairly new and unusual welding technique, thus critical information about the nomenclature is presented below:

Tool Shoulder: is the wide diameter section that is in contact with the top surface of the workpiece. Temperature level is mainly controlled by the tool shoulder, as the shoulder applies the downward force combined with rotation, creating the frictional heating effect [Rambabu et. al., 2015]. In addition to temperature, tool shoulder is also responsible for applying the necessary pressure onto the workpiece and containing the plasticized material underneath itself. Because of these reasons, tool shoulder has crucial importance on the FSW process and outcome. Diameter of the tool shoulder is vital, and it may have concave, convex and flat surfaces.

Tool Pin: is the part that is inserted into the workpiece and traversed inside of it during welding. Tool pin also contributes to heating, however its main function is to 'stir' the welding zone. It creates huge plastic deformation in the weld zone and mixes the material between two sides. The plastic deformation by the pin results in fine grain microstructure in the weld nugget. Pins can have different shapes such as; cylindrical, conical, threaded, fluted etc.

Tool Rotation Rate: is the RPM, which the FSW tool is turned at. This parameter impacts the heat input and material flow.

Tool Advancing Speed: is the speed in which the FSW tool travels. This parameter has importance on the thermal cycle that is experienced by the workpiece and current welding region since it controls the weld time for the given heat input rate.

Tilt Angle: is the angle between the normal to the workpiece and FSW tool shaft. This angle is typically kept between 0 and 3 degrees. Tilt angle is important for the containment of the plasticized material flowing underneath the tool.

Plunge Rate: is the rate at which the tool drills/enters into the workpiece at the beginning of the process.

Plunge Depth: is the depth that the tip of the tool pin reaches from the top of the workpiece surface. FSW machines can be programmed to control and keep this position of the tool fixed throughout the welding operation.

Axial Force: is the vertical downward force the tool applies on the plates to be welded. This force creates the normal force required for the friction, as well as the pressure for the deformation bonding. FSW machines can be programmed to control and keep this force level fixed throughout the welding operation.

Metallurgical benefits	Environmental benefits	Energy benefits
Solid phase process	No shielding gas required	Improved materials use (e.g., joining different thickness) allows reduction in weight
Low distortion	Minimal surface cleaning required	Only 2.5 % of the energy needed for a laser weld
Good dimensional stability and repeatability	Eliminate grinding wastes	Decreased fuel consumption in light weight aircraft, automotive and ship applications
No loss of alloying elements	Eliminate solvents required for degreasing	
Excellent mechanical properties in the joint area	Consumable materials saving, such as rugs, wire or any other gases	
Fine recrystallized microstructure	No harmful emissions	
Absence of solidification cracking		
Replace multiple parts joined by fasteners		
Weld all aluminum alloys		
Post-FSW formability		

Figure 1.3: Advantages of Friction Stir Welding [Mishra et. al., 2014].

As a solid-state process, FSW doesn't consume any filler material and it doesn't contain any melting phase. Because of these properties, one doesn't have the concerns of solidification cracking, chemical compatibility, and post-weld heat treatability with FSW, which are problematic issues for fusion welding. All aluminum alloys can be welded with FSW as well due to these advantages.

FSW process has excellent post-weld mechanical properties since the weld zone can have as high as 85-90% mechanical strength of the base metal. In addition, because there is no filler material involved, with appropriate post-weld heat treatment the weld zone hardness can be recovered to its original base metal state. These supreme features enable parts that are joined with FSW to be lighter, stronger, have complex geometries, and have less constraints on the materials to be used, compared to fusion welding and other joining techniques.

Before FSW, there were other ‘friction welding’ techniques, such as ‘rotary friction welding’, ‘linear friction welding’. However, in previous techniques geometries of the parts to be welded were constrained, mostly parts were needed to be symmetrical or cylindrical. In FSW, especially with the use of a 6-axis robotic arm, complex geometries and formed surfaces or paths can be joined, making FSW suitable for many different sectors and applications.

Trains, shipbuilding, automobiles, aerospace applications and many more utilize friction stir welding. A few examples to recent use cases are; Chinese high speed trains, both sides of iMac monitor, body parts of Ford GT etc.

Among the broad range of applications and sectors, aerospace industry is the fastest one to implement this technology in its operations. The main appeal for the aerospace industry was the advantage of FSW enabling to join all aluminum alloys, especially 2XXX and 7XXX aluminum alloys [Langari et. al., 2016]. These alloys were desired for their high strength and good mechanical properties, however, couldn’t be joined with the current techniques until the arrival of FSW. These alloys are especially used in aerospace industry for pressurized chemical vessels. Due to the large diameter and high ‘maximum allowable operating pressure’ (MAOP) needs from these pressure vessels in space and rocket applications, current manufacturing and joining techniques were limiting the capabilities, preventing 2XXX and 7XXX high-strength aluminum alloys to be used as they were labeled ‘nonweldable’. After the introduction of FSW these limits were lifted as new possibilities opened up for the industry and new heights have been reached ever since.

CHAPTER 2:
LITERATURE REVIEW

Since the introduction of FSW in 1991, there have been research on the topics of; the effects of process parameters on the weld, post-weld heat treatment, tool design, microstructural formation, joining dissimilar materials, weld plate and path configuration etc. Although there is a wide range of topics that are investigated throughout the years, most of them happen to be case specific since there is numerous combinations of different materials or parameters, so there are still huge gaps in the current literature. Certain aspects of FSW process to this day are still unclear, such as material flow inside the weld nugget. All attempts and new studies increase the collective knowledge around the FSW process and make it more completely understood.

Cao and Kou investigated the material phase inside the weld zone for Al 2219 by looking at the microstructures of the weld for Θ (Al_2Cu) particles. FSW process is conducted at below near melting temperature and if the process parameters are not well chosen, heat input cannot be controlled optimally, resulting in liquification of metal. Researchers have used Θ particles as in-situ microsensors to see if liquification occurs during their process. Al 2219 has a lower bound of melting temperature which is also its eutectic temperature at 548^{o}C making it ideal for observing the post-weld microstructure for signs of liquification. They used gas metal arc welding (GMAW), which includes a liquification process, to confirm if the Θ particles are present when the metal melts in the weld zone. Looking at the post FSW microstructure of the material, no eutectic particles were found in the weld zone indicating that no liquification occurred during the process [Cao et. al., 2005].

Langari, Kolahan and Alakbari conducted research on the effects of tool rotation rate and advancing speed on the mechanical properties of Al 7075 – T651 plates. In order to evaluate the outcome of the weld; microhardness, weld morphology, elongation and tensile properties of the test specimens were investigated. Their results indicated that as the advancing speed increased for the same rotational rate, the axial force and microhardness of the weld zone increased however, the quality of the weld appearance decreased. This is a common trade-off in FSW process as, less heat input and more aggressive deformation resulting in finer grain microstructure and mechanical properties but increasing the risk of weld to be not joined completely and decreasing the weld quality. They also observed that increasing the rotational rate did not affect the axial force and weld morphology as much as advancing speed. They also found that increasing the tilt angle from 0^0 to 2.5^0 resulted in better weld morphology [Langari et. al., 2016].

Fujii et. al. worked on the effects of the tool shape on the mechanical properties and overall weld quality for aluminum alloys. They used a straight columnar pin geometry, threaded columnar pin geometry and triangular prismatic pin geometry with same shoulder diameter. Aluminum alloys utilized for this research were Al 1050 – H24, Al 6061 – T6 and Al 5083 – O. For Al 1050 and 6061 alloys it was found that straight columnar tools worked best as both these alloys have low deformation resistance. Good weldability of Al 6061 also makes it suitable to work with less aggressive tool dimensions and with a broader range of parameters than other aluminum alloys. On the other hand, it was found that for Al 5083 which has a higher deformation resistance, triangular prismatic and threaded columnar geometries worked best as these tools increased deformation in the weld zone [Fuiji et. al., 2006]. Findings of this study are in accordance with current state-of-the-art because it is widely accepted among friction stir welding tool manufacturers and welders that a conical threaded pin with flutes result in best results. An example of such a tool can be found in the figure below, which is the production of the founders of friction stir welding, TWI. Ridges on the shoulder have critical importance as well for containing the weld material underneath the tool and swage it on the surface.

Figure 2. 1: Triflute Tool Prototype [Kallee et. al., 2001].

J. Boonma et. al. investigated the post-weld heat treatment effects on friction stir welded Al 6061 – T651 specimens. Findings are impressive in the sense that with PWHT, researchers accomplished to recover the strength of the weld zone to base metal levels. PWHT of the samples were carried out first by solution heat treatment, followed by quenching and aging with different parameters. To assess the results hardness values were taken from the cross section of samples. Hardness and tensile strength were found to be closely correlated as well. Hardness values of the as welded nugget and thermo-mechanically affected zones were found to be about 74 VHN, while the base metal was around 116 VHN.

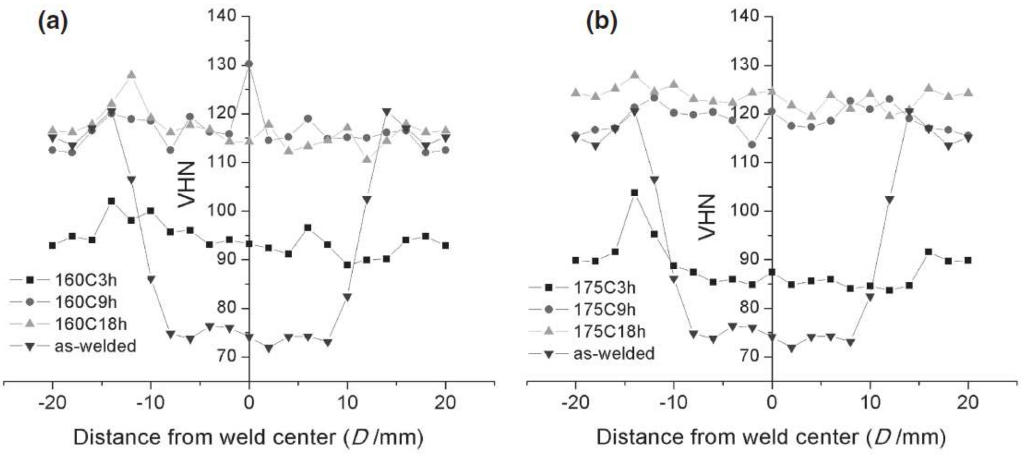

Figure 2. 2: J. Boonma et. al. Hardness values of as welded and PWHT Samples [Boonma et. al., 2015].

Figure 2.2 shows some of the results of J. Boonma et. al. work as different PWHTs were applied on samples. Hardness profile of the as-welded samples show a 'U' shape behavior because of the softening effect on nugget zone and TMAZ. However, PWHT procedures work well as heat treated and aged samples recover their full hardness and become uniform with the base metal. This effect is expected since there is no filler material in FSW process, thus heat treatment following the welding operation affects particles homogeneously. As a result of PWHT fully joined Al 6061 samples are able to be recovered to their former mechanical properties, and in some cases even improving due to heat treatment [Boonma et. al., 2015].

Findings of J. Boonma et. al. are crucial for high demand applications such as automotive and aerospace industry. Absence of a filler material enables the joint line to be post-weld heat treated to a mechanical level that can be called 'original material' or even higher properties than original. In future works of this thesis, a liquid oxygen oxidizer tank is attempted to be stir-welded for hybrid rocket applications. For better mechanical strengths, higher strength-to-weight ratios heat treatment and alloy strength are crucial and being able to PWHT a pressure vessel enables engineers to achieve higher performance metrics.

CHAPTER 3:
FSW PROCESS DYNAMICS

FSW process is a metal joining process that incorporates plastic deformation and diffusion bonding. To accomplish these solid-state bonding phenomena, FSW process mainly utilizes heat. Heat is created via frictional heat on the contacting surfaces of the tool and the workpiece.

There are two main phases of FSW process, which are:

a) Plunge and dwell phase
b) Traverse and welding phase

When both the tool and workpiece is at ambient temperature, the tool is slowly plunged into the workpiece while rotating at high RPM. During this stage the tool is inserted into the workpiece initially by a drilling motion and it gets easier to penetrate as tool pin surface heats up the contact space. Vertical force between the tool and the workpiece peaks with the first contact of the tool pin tip and workpiece and it drops down as the zone heats up. As the tool pin gets submerged in the workpiece, plunge phase comes to an end.

A second peak in the vertical force is observed at the end of the plunge phase when the tool shoulder touches the workpiece. Tool shoulder is the main contributor to the frictional heat generation since it has the largest surface area. Tool shoulder generally plunges by 0.05 – 0.2 mm to the workpiece and the vertical motion of the tool stops while it is rotating. At this phase dwelling occurs where the second peak downward force starts to drop down with the temperature rise in the material caused by the frictional heating that is caused by the large shoulder area of the tool.

Dwelling phase is much quicker compared to the plunge phase, where the tool is slowly submerged into the workpiece. With entire tool pin and tool shoulder plunged into the workpiece while rotating, the workpiece heats up due to frictional heating and the workpiece gets plasticized and reaches to the required temperature for the plastic flow.

As the tool-workpiece interface gets heated up to the requirements, the tool starts its advancing motion along the weld line. Most applications use a downward force-controlled machine during this phase in order to control the heat input. Tool creates downward force on the workpiece to create frictional heating as well as to push down the plasticized metal to force bonding. In addition to this, the heat created by the shoulder and the tool pin submerged in the workpiece plasticizes the metal around the pin and creates material flow between two joining sides of the weld seam.

First the friction created between the tool and the workpiece can be shown as below:

$$F = \mu * P \qquad (3.1)$$

F = frictional force

μ = coefficient of static/dynamic friction

P = normal force

If we divide the two sides of the equation by area, we get the coulomb friction as

$$T = \mu * p \qquad (3.2)$$

T = shear stress

p = pressure

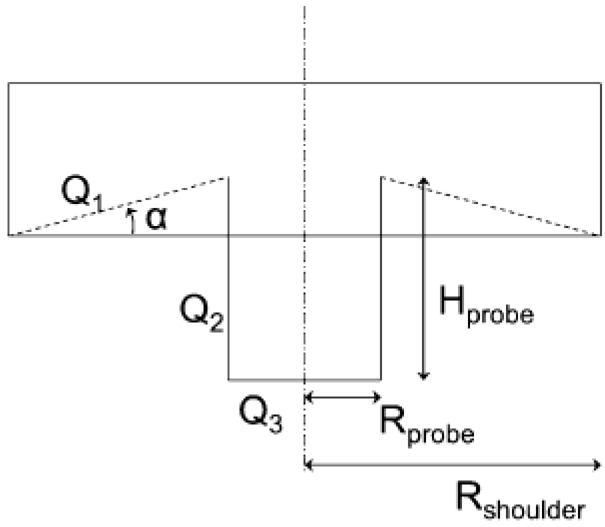

Figure 3. 1: General Shape of a Tool with Conical Shoulder Surface [Mishra et. al., 2014].

There are three zones on the tool that contributes to the frictional heating, which can be seen in the figure below: (a) tool pin tip, (b) tool pin cylindrical surface, and (c) concave conical surface of the tool shoulder.

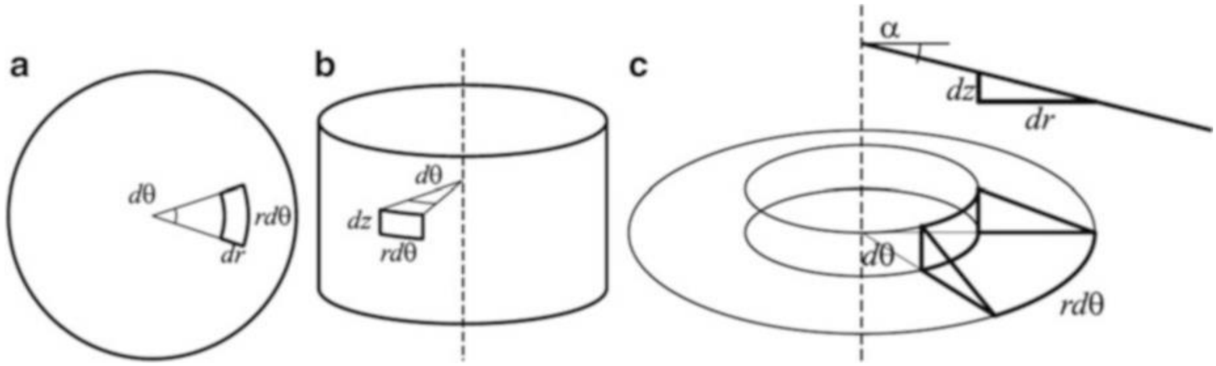

Figure 3. 2: Infinitesimal Elements of Different Frictional Heating Contributors on the Tool [Mishra et. al., 2014].

The general principle governing the frictional heat at these zones is:

$$dQ = w * r * dF \tag{3.3}$$

dQ = heat generated per unit time

w = angular velocity of the tool

r = distance from the tool centerline

dF = force acting on the surface

Different segments of the tool that contribute to the frictional heating are:

Qa = heat generated at the tool pin tip

Qb = heat generated at the tool pin cylindrical surface

Qc = heat generated at the tool shoulder

For Qa, the infinitesimal area can be shown as $dA = rd\theta dr$. By dividing the dF with dA,

$$dQa = w * r^2 * Tshear * d\theta * dr \tag{3.4}$$

By integrating this equation over the tool pin tip area,

$$Qa = \int_{r=0}^{Rpin} \int_{\theta=0}^{2\pi} \omega \cdot r^2 \cdot \tau_{shear} \cdot d\theta \cdot dr$$

$$Q_a = \frac{2}{3} \pi \tau_{shear} \omega R_{pin}^3$$

For the cylindrical portion of the pin surface the infinitesimal area is as below:

$$dA = rd\theta dz$$

z is the axial direction of the pin. This area is acted by $Tshear$ and the differential tangential force to the pin surface can be found by multiplying the two. After that, by multiplying this value with the radius of the pin and the angular velocity, one can reach to the heat generated by the cylindrical surface of the pin as:

$$dQb = w * r^2 * Tshear * d\theta * dz \quad (3.5)$$

By integrating the above over the cylindrical surface of the pin:

$$Qb = \int_{\theta=0}^{2\pi} \int_{z=0}^{Hpin} \omega \cdot r^2 \cdot \tau_{shear} \cdot d\theta \cdot dr$$

$$Q_b = 2\,\pi\,\tau_{shear}\,\omega\,R_{pin}^2$$

Lastly, the shoulder creates the largest heat generation during the process. If the surface has a conical face than the angle with the parallel surface should be taken into consideration, which is ‘α’. The infinitesimal area of the shoulder surface can be found as below:

$$dA = rd\theta(dr + dz) = rd\theta(dr + dr\,tan\alpha) = rd\theta dr(1 + tan\alpha)$$

This infinitesimal area on the shoulder surface of the tool is acted by $Tshear$ and this interaction creates the largest generation between the contact surfaces due to its large shoulder area. Heat generation of the shoulder surface can be found as below:

$$dQc = w * r^2 * Tshear * (1 + \tan(\alpha)) * dr * d\theta \quad (3.6)$$

Integrating the above over the conical surface of the tool shoulder

$$Qc = \int_{r=Rpin}^{Rshoulder} \int_{\theta=0}^{2\pi} \omega \cdot r^2 \cdot \tau_{shear} \cdot (1 + \tan(\alpha)) \cdot dr \cdot d\theta$$

$$Q_c = \frac{2}{3}\pi(1 + \tan(\alpha))\tau_{shear}\,\omega\,(R_{shoulder}^3 - R_{pin}^3) \quad (3.7)$$

In this work, the tool used for stir welding applications has no conical surface on the shoulder so the conical shoulder surface angle α can be taken as ‘0’. This provides simplicity for manufacturing aspect as well as the economical aspect of tool making. Due to this, Eq. 3.7 simplifies to:

$$Q_c = \frac{2}{3}\,\pi\,\tau_{shear}\,\omega\,(R_{shoulder}^3 - R_{pin}^3)$$

Since the largest heat generation happens on the surface of the shoulder the heat generation from the cylindrical surface can be ignored for simplicity. Adding the heat generation caused by the tool pin tip to this equation, one can get a more simplified equation for the heat generated by the tool as:

$$Q_{gen} = \frac{2}{3}\,\pi\,\tau_{shear}\,\omega\,(R_{shoulder}^3) \qquad (3.8)$$

CHAPTER 4:
METHODOLOGY

In this thesis, 5 mm Al6061 – T6 plates were investigated to be joined by friction stir welding. A threaded conical pin with four flutes and a flat shoulder surface was designed from H13 tool steel to be used as the FSW tool. A force controlled 'China FSW Center' Gantry Model Friction Stir Welding Machine was used to conduct the FSW operations.

An empirical approach is aimed to determine a function that relates several FSW parameters to mechanical properties of the material, such as ultimate tensile strength (UTS), yield strength in un-aged and aged conditions post-welding. To do so, a 'Full Factorial Design' of experiment set was determined and the result of the tests were analyzed through 'Response Surface Methodology'.

In this chapter, first the plate preparation and tool-fixture design will be elaborated. Then the test parameters and the post-weld processing of the plates will be explained. Lastly, the techniques and approach used for response surface methodology and fracture mechanics will be introduced.

4.1 Plate Preparation

First, aluminum plates checked via metal spectrometer prior to welding. The chemical composition of the material was confirmed to be Al6061.

Figure 4. 1: Metal Spectrometer.

Then the plates were machined to the designed dimensions. Initially the aluminum plates were surface machined to 6,3 mm for welding phase. Sides of the plates were also machined in order to acquire perfect matching for the butt weld joint. Plates were chosen approximately

25% larger than the final thickness in order to eliminate root and surface flaw mechanisms as it can be seen in Fig. 4.2. The plates were machined down to 5 mm, reducing 0,65 mm from upper and lower surfaces, after the welding was complete.

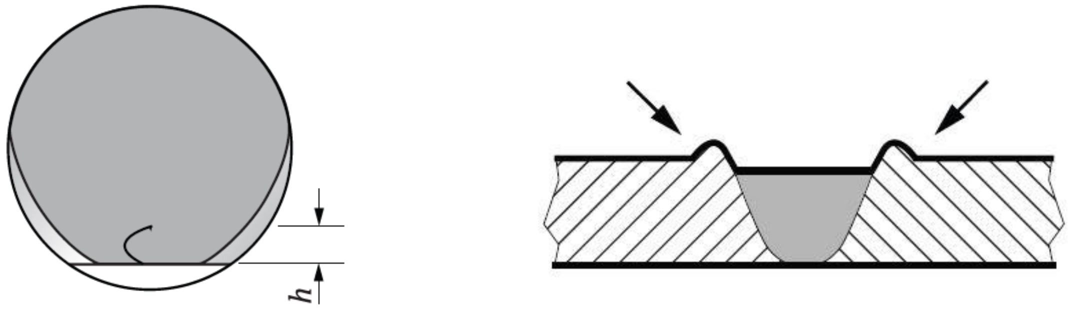

(a) (b)

Figure 4. 2: Flaw Mechanisms: (a) Root Flaw, (b) Toe Flash [ISO, 2020].

Plates were also machined on sides to get perfect dimensional accuracy and merging of the butt weld joint surfaces. The dimensions of the individual plates prior to joining were 100mm x 185mm x 6,3mm.

Figure 4. 3: Plate Dimensions.

4.2 Tool-Fixture Design and FSW Machine

A tool with a pin geometry of tapered threaded, four flute, conical pin with flat shoulders were designed for the FSW tool. Tool material was chosen to be ‘H13 Tool Steel’ for its hot hardness and high strength mechanical properties. Tool shoulder was 15 mm in diameter and conical pin diameters were 5 mm and 3 mm from top to bottom. Pin length was 6 mm which is 95% of plate thickness as it is in accordance with literature.

Figure 4. 4: FSW Tool.

Figure 4. 5: FSW Fixture.

Plates were pressed down onto the FSW machine table with six clamping jaws and two side jaws. Initially a fixture was designed to acquire load cell measurement from the bottom of the plates and to retain the plates from the sides, as the designed fixture can be seen in Fig. 4.6. This design was developed for a non-force-controlled CNC machining center, and it can be used in applications where a force controlled FSW machine is not available. However, the force control of the FSW machine was in 1% accuracy so load cell was not needed. Additionally, the rectangular housing of the plates was found to be unnecessary after initial trial tests, so further operations were conducted with an easier fixture as in Fig. 4.5.

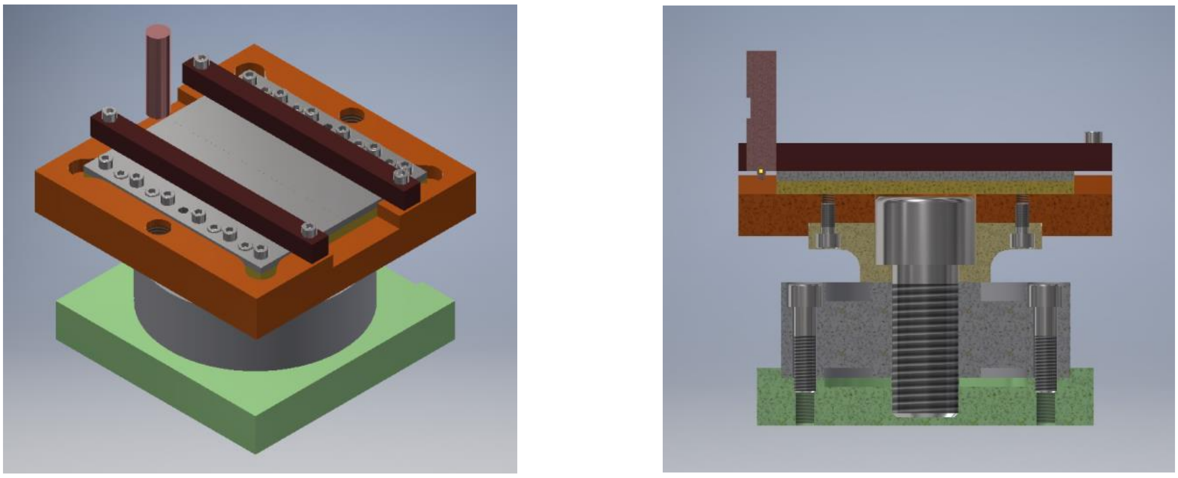

Figure 4. 6: FSW Fixture Design for CNC Machine.

Figure 4. 7: FSW Machine.

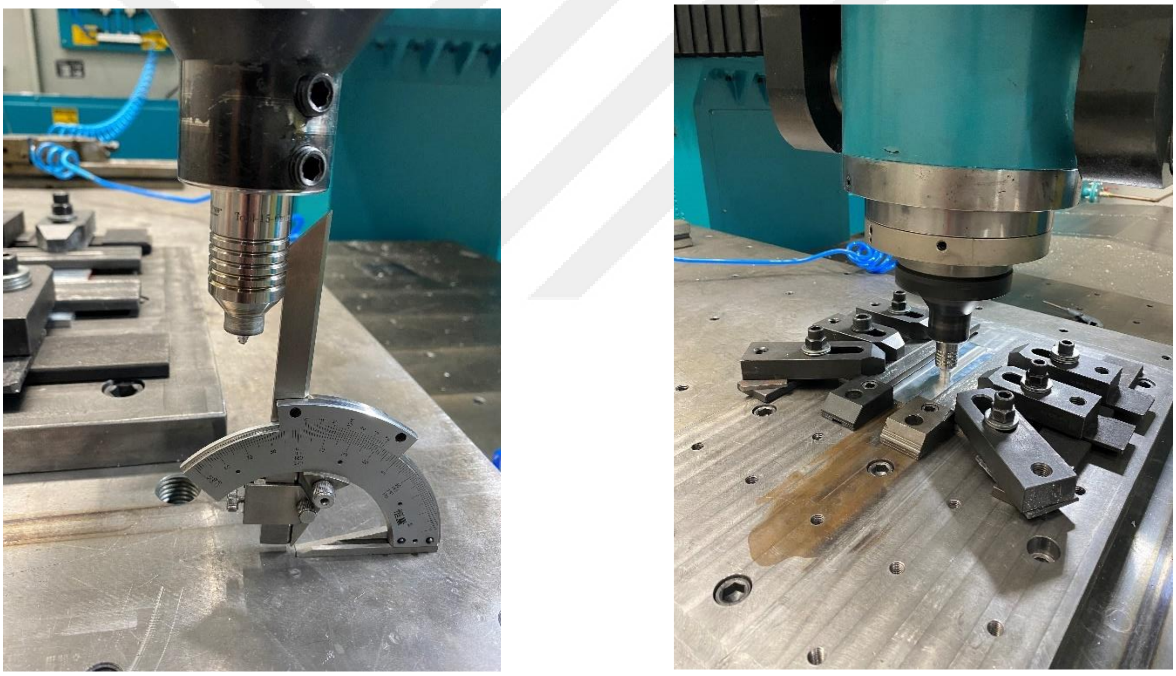

Figure 4. 8: Tilt Angle Setup and FSW Process.

Tests were conducted on the ‘Gantry Model FSW Machine’ developed by ‘BEIJING FSW TECHNOLOGY CO., LTD.’. Model type is ‘FSW-LM-BM16-2D’. This model was specially developed for welding of aluminum alloys between 1-16 mm thickness. Strokes of axes are; X-2300 mm, Y-1500mm and Z-300 mm. Tool head has ±5° tilting capability.

4.3 Experimental Design and Welding Parameters

FSW tests were designed to acquire an empirical formula relating major friction stir welding parameters to test specimen’s mechanical properties. To do so, main contributing parameters were determined from literature and past experiments as: rotational speed, welding(traverse) speed and down force. Ranges of these parameters were determined to cover the large spectrum of appropriate values:

Table 4. 1: Variable Values of Welding Parameters.

	Low	**Medium**	**High**
Rotational Speed [RPM]	900	1400	1900
Welding Speed [mm/min]	300	500	700
Down Force [N]	3000	3500	4000

Full factorial design of experiments was determined and a total of 27 tests were conducted as a combination of the three values of the aforementioned major contributing parameters. Other parameters such as; tilt angle, dwell time, plunge rate were kept constant throughout all tests.

Table 4. 2: Constant Welding Parameters of the Process

Dwell Time [s]	10
Plunge Rate [mm/min]	18
Tilt Angle [°]	2,5

4.4 Post-Processing of Plates

After the welds were complete, hardness measurements were taken on the upper surface along the joint line as it can be seen in Fig. 4.9.

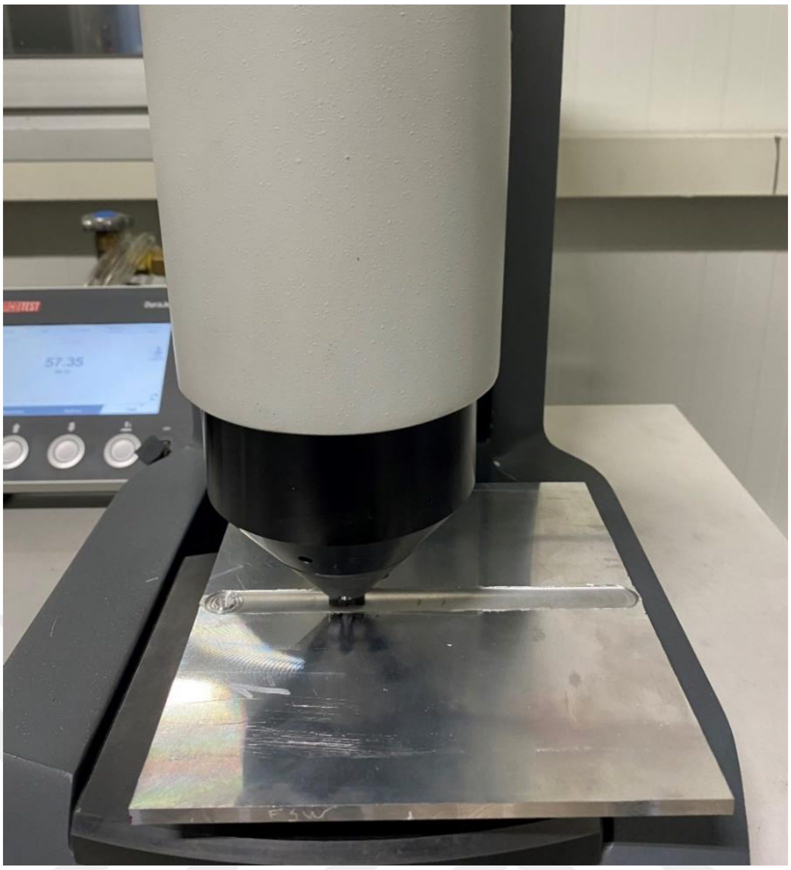

Figure 4. 9: Hardness Measurements.

Hardness values were taken from the base material as well and it was found to be 102-103 HB.

Table 4. 3: Full Factorial Design and Hardness Values.

		Rotational Speed [RPM]	Welding Speed [mm/min]	Down Force [N]	Hardness of Weld Surface [HB]
FSW-01		900	300	3000	55, 59, 57
FSW-02		900	300	3500	57, 60, 59
FSW-03		900	300	4000	59, 59, 60
FSW-04		900	500	3000	58, 58, 59
FSW-05		900	500	3500	57, 59, 58
FWS-06		900	500	4000	58, 59, 58
FSW-07		900	700	3000	57, 55, 56
FSW-08		900	700	3500	55, 58, 58

FSW-09		900	700	4000	58, 59, 60
FSW-10		1400	300	3000	55, 54, 55
FSW-11		1400	300	3500	54, 55, 55
FSW-12		1400	300	4000	54, 55, 55
FSW-13		1400	500	3000	60, 59, 61
FSW-14		1400	500	3500	58, 59 , 59
FSW-15		1400	500	4000	61, 62, 60
FSW-16		1400	700	3000	61, 60, 60
FSW-17		1400	700	3500	60, 61, 60
FSW-18		1400	700	4000	61, 62, 59
FSW-19		1900	300	3000	57, 56, 55
FSW-20		1900	300	3500	54, 56, 55
FSW-21		1900	300	4000	56, 55, 54
FSW-22		1900	500	3000	58, 56, 57
FSW-23		1900	500	3500	60, 58, 59
FSW-24		1900	500	4000	59, 60,58
FSW-25		1900	700	3000	53, 55, 54
FSW-26		1900	700	3500	50, 51, 50
FSW-27		1900	700	4000	49, 48, 49

Hardness values of the weld region drops expectedly, since the high temperatures (>450°C) achieved in weld region causes fine needle shaped precipitates (which are strengthening agents in 6xxx aluminum alloys) to dissolve, as this softens the material [Woo and Choo, 2011].

After the hardness measurements were taken from the upper surface of the plates, radiographic image of all the test plates were taken to see if there is any defect present inside the weld zones. No defects were found in the plates except FSW-07-08-09 plates.

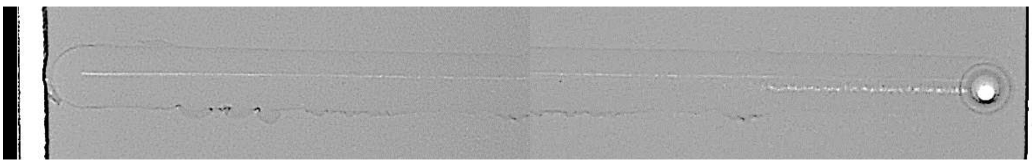

Figure 4. 10: Radiographic Image of FSW-07 Plate.

The plates were then surface machined down to 5 mm, taking 0,65 mm from each surface. Machined plates were then cut by water jet cutter to extract tensile test and bending samples. The samples were taken perpendicular to the weld line. The placement of the samples can be seen in the CAD arrangement figure down below.

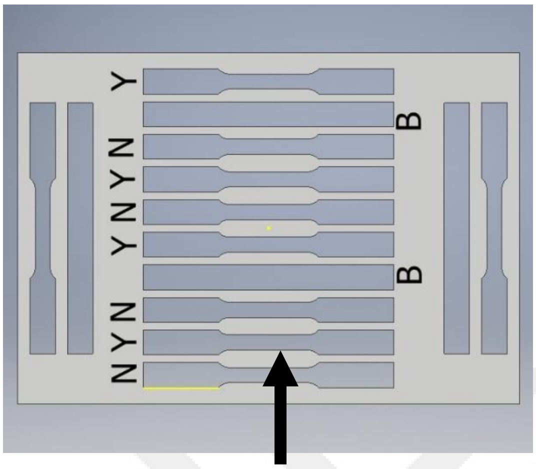

Figure 4. 11: Sample Layout.

Along the weld direction (shown with the arrow), 15 mm portions were removed in order to discard the entry and exit points of the FSW tool [ISO, 2020]. Total of eight tension samples were cut along the weld line, four of them were to be tested directly, and four of them to be tested after 8-hour aging process at 180°C. So, there were an aged group and un-aged group of specimens for both tensile testing and metallographic investigation. This was done to see the precipitation hardening effects of Al6061 on FSW samples and to reach better mechanical properties. Discussion is taken into more depth with the comparison of aged and un-aged specimens.

Tension test samples were marked on the plates according to their placements and then were tested on Shimadzu 100kN tensile test machine.

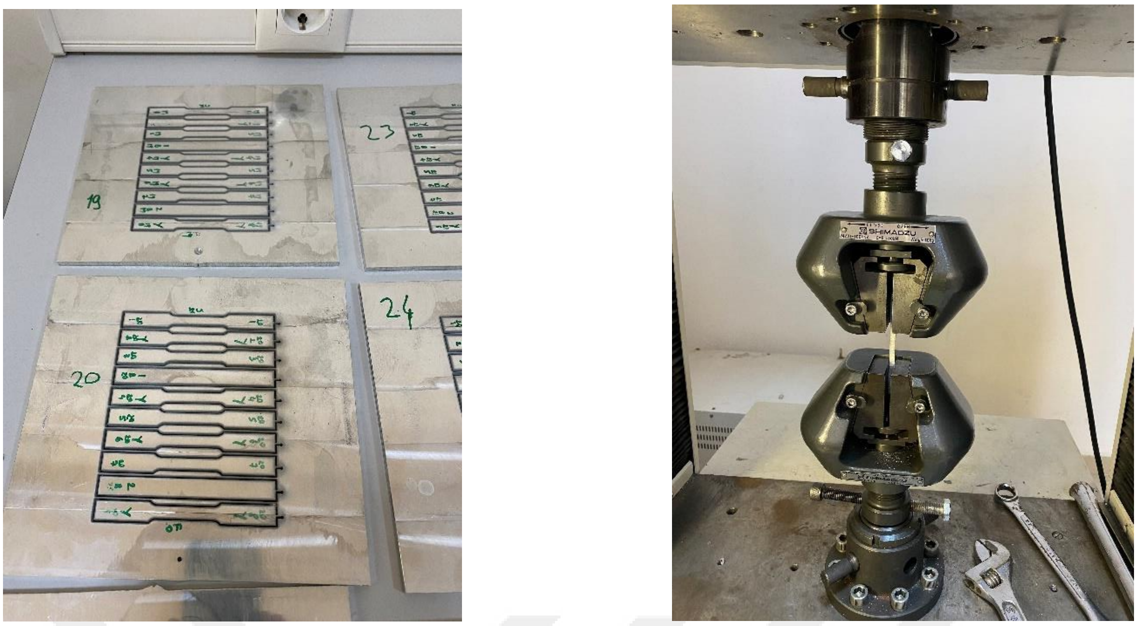

Figure 4. 12: Tensile Tests.

4.5 Response Surface Methodology

In a process, when the relation between the controllable variables and an outcome are too complex to physically model, and empirical approach needs to be taken to configure the problem. Response Surface Methodology (RSM) provides an effective and powerful tool for these kinds of problems where one wants to observe the effects of a set of factors (controllable variables) on responses (outcomes). The main goal of the method is to use the experimental data and fit a model to this, to predict the region in and out of the experimental domain range as accurately as possible. In addition to this RSM shows the interrelations of different factors combined with each other, resulting in a greater analysis [Sarabia and Ortiz, 2009]. FSW process is a highly complex technique that the RSM approach is suitable for.

To conduct RSM one must create a design of experiments and determine the factors and responses.

4.5.1 Full-Factorial Design

Most widely used experiment designs, especially in manufacturing fields are full and fractional factorial designs. These designs can be conducted in 2-levels and 3-levels. A full factorial design of experiment consists of all possible combinations of the factors with each other on all levels. This factorial design approach also enables to observe the joint effect of the controllable variables on the desired outcomes [Antony, 2014]. For the scope of this study, a full factorial design with 3-levels was chosen. The set of experiments can be seen below.

Table 4. 4: Full Factorial Design of Experiments.

		Rotational Speed [RPM]	Welding Speed [mm/min]	Down Force [N]
FSW-01		900	300	3000
FSW-02		900	300	3500
FSW-03		900	300	4000
FSW-04		900	500	3000
FSW-05		900	500	3500
FWS-06		900	500	4000
FSW-07		900	700	3000
FSW-08		900	700	3500
FSW-09		900	700	4000
FSW-10		1400	300	3000
FSW-11		1400	300	3500
FSW-12		1400	300	4000
FSW-13		1400	500	3000
FSW-14		1400	500	3500
FSW-15		1400	500	4000
FSW-16		1400	700	3000
FSW-17		1400	700	3500
FSW-18		1400	700	4000
FSW-19		1900	300	3000
FSW-20		1900	300	3500
FSW-21		1900	300	4000
FSW-22		1900	500	3000
FSW-23		1900	500	3500
FSW-24		1900	500	4000
FSW-25		1900	700	3000
FSW-26		1900	700	3500
FSW-27		1900	700	4000

4.5.2 Determination of Parameter Ranges

The parameter ranges of the factors were chosen from literature and past experiments. The values were chosen to be extensive enough to cover a large portion of the applicable parameter spectrum. In addition to this, the limits were also determined to acquire sound welds from almost all the experiments. This was crucial to include as much data point as possible without the erroneous results caused by defects in the weld.

Main factors were chosen as; rotational speed (RPM), welding speed and down force. RPM and down force are the two main contributing factors to the heat rate caused by the tool. Welding speed is the third factor that affects the heat in a different sense that it determines the weld time, thus resulting in longer or shorter amount of time that the weld zone is exposed to heat. These factors create and control frictional heating which changes the microstructure especially in the HAZ and TMAZ regions.

In addition to heat effects, determined factors also control the mixing of the weld nugget zone and plastic deformation bonding mechanisms. These effects result in different shapes of the TMAZ and weld nugget zones, which changes the fracture mechanism of the test specimens. These mechanisms play a crucial role in the type of failure and strength of the fracture zone, and are vital to understand to control and improve the weld zone. The ranges of the parameters for the determined factors are summarized in the table below.

Table 4. 5: Range of Parameters.

	Unit	**-1**	**0**	**1**
Rotational Speed	[RPM]	900	1400	1900
Welding Speed	[mm/min]	300	500	700
Down Force	[N]	3000	3500	4000

4.5.3 Responses

To analyze the effects of RPM, welding speed and down force as factors; yield strength, ultimate tensile strength and maximum strain were chosen as responses for the mechanical behavior criterions.

Yield Strength

Yield strength is the strength limit that the material can go through deformation without permanent effects. This limit separates the elastic and plastic deformation regions and yielding starts after additional load is applied to the material past yield strength. In some applications for metals this point is considered to be the failure limit. Especially in pressure vessel manufacturing the design limit is taken to be the yield strength. Yield strength is directly proportional to the stiffness of the material.

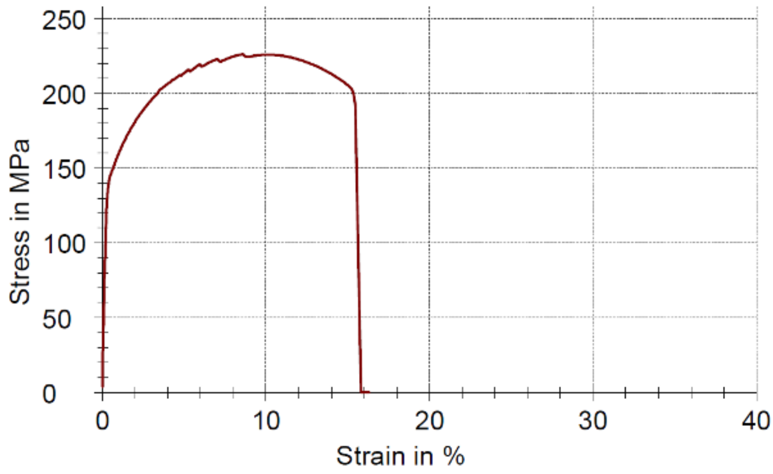

Figure 4. 13: FSW-13-07 Stress Strain Curve

It can be seen in Fig. 4.13 that after 143 MPa the material reaches its yield strength and plastic deformation begins.

Ultimate Tensile Strength

Ultimate tensile strength or UTS is the maximum stress or load that the material can withstand before failure. This failure can be in fracture or necking as the material continues to strain but the load carrying capability of it is mostly diminished after passing UTS. The UTS point can be seen in Fig. 4.13 as 226 MPa.

Strain at Maximum Load

Maximum strain or elongation is the deformation capability of the material before failure. Maximum strain is 8,19% for FSW-13-07 test specimen. This parameter is extremely important because strain gives the toughness or energy absorption capability of the material. Without any strain capability even a high UTS material would fail when faced with a stress concentration region in the material or shock load.

Regression Analysis

Regression analysis was conducted on Stat-Ease 360, as it analyzes the data in accordance with the response surface method. Then the least significant factors were eliminated, which was decided by a significance level of 0,05. Each factor having a p-value higher than 0,05 were eliminated from the model.

4.6 Microscopy

In addition to tensile testing, metallographic examination was conducted. In this step the weld quality was observed as well as the microstructure in different weld zones. In these different weld zones particular shapes were observed in the distribution of microstructure, which might affect the failure mechanism and crack initiation. These shapes also change with varying process parameters. Tool shape might have a significant effect on these shapes.

For microstructure observations, metallography samples were first cut in correct sizes and then grinded and polished. After the polishing phase observed surfaces were etched with Keller's reagent and put under stereomicroscope (10x) and optical microscope (50x).

After the tensile testing, fracture surfaces of the tensile test specimens were investigated to analyze the fracture zones, crack propagations, microstructure distribution and overall fracture mechanism. These analyses were conducted with 'Celestrone Micro-Direct Digital Microscope'.

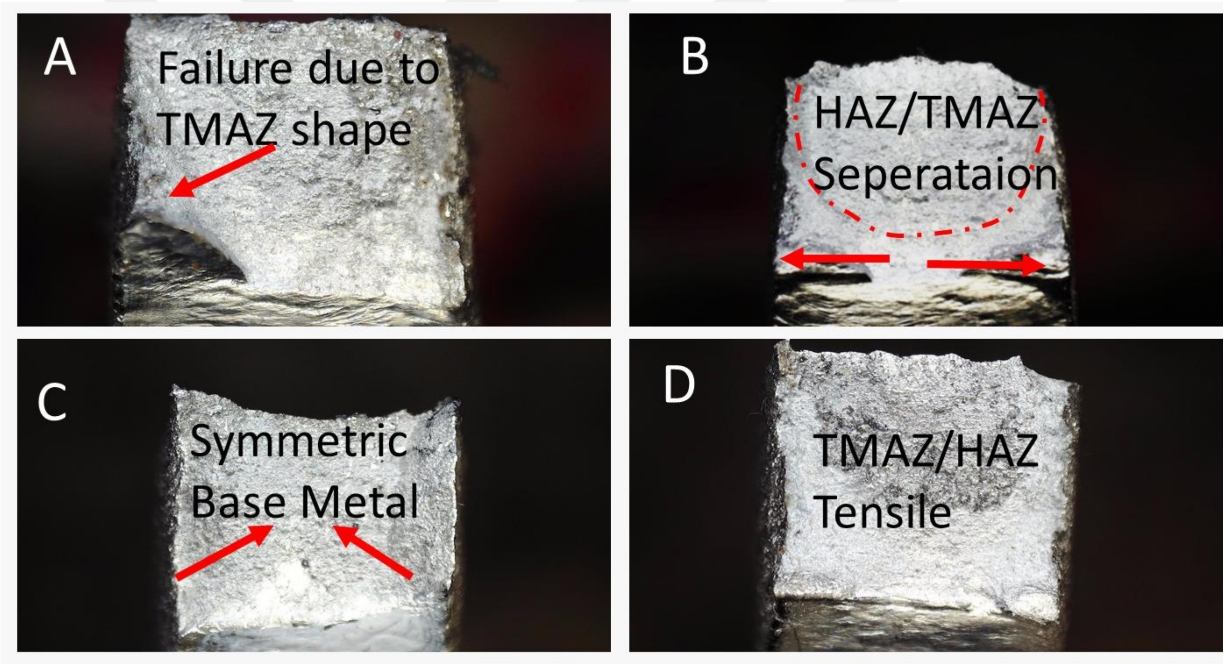

Figure 4. 14: Different Fracture Zone Types.

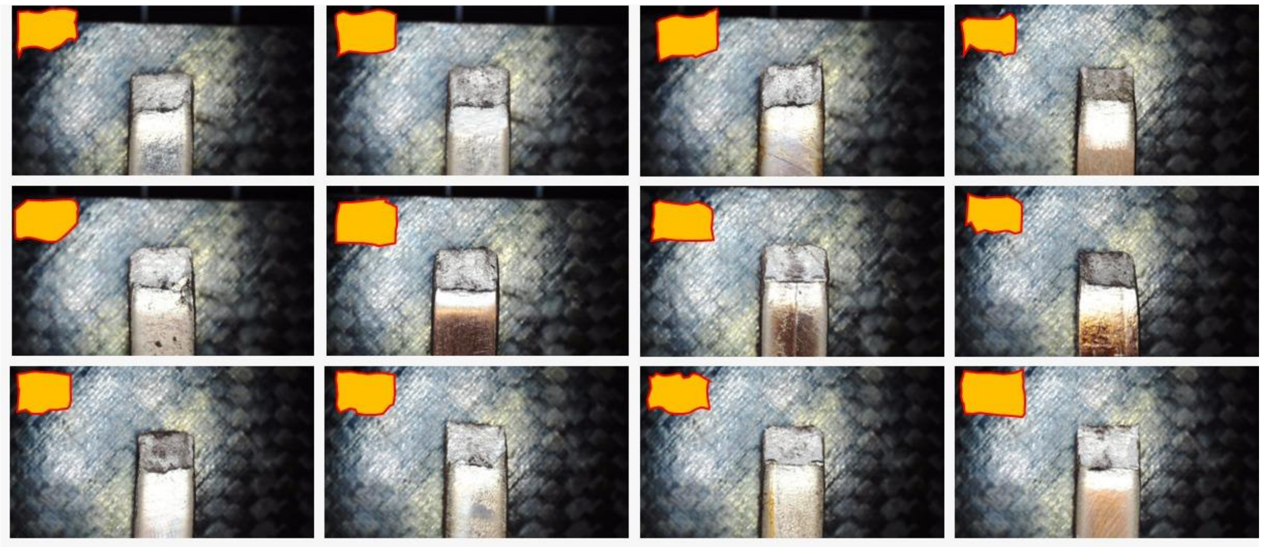

Figure 4. 15: Top Views of Fracture Surfaces.

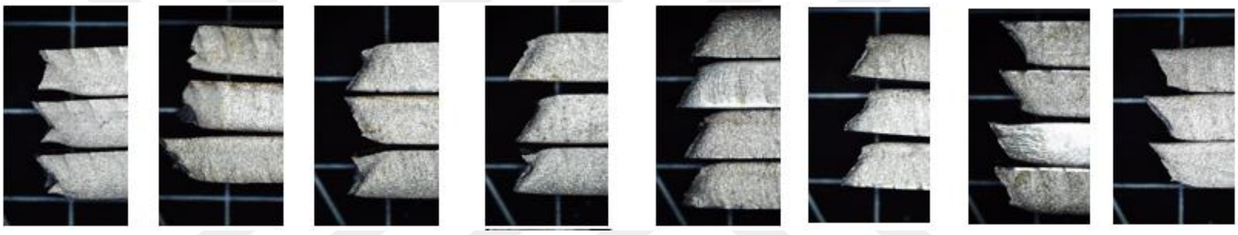

Figure 4. 16: Side Views of Fracture Surfaces.

Fracture surfaces were analyzed for all specimens, by taking the fracture surface, top view and side view images and analyzing them under the microscope. Two main fracture zones were identified: weld zone and TMAZ-HAZ region. These varying fracture zones result in different mechanical properties especially for strain capability of the material.

CHAPTER 5:
RESULTS AND DISCUSSION

5.1 Data Evaluation and Grouping

To portray the data distribution and differences between the tested samples, for un-aged specimens, the whole data used in full factorial design was used to separate samples into regions according to their maximum stress and maximum strain values. As depicted in Fig. 5.5, samples were divided into two categories. A low-stress low strain (Group A) and a high stress-high strain region (Group B). An interesting fact however was that for Group A specimens, values existed high variance in stress ranging from 120 MPa to 220 MPa whereas for Group B stress values were clustered around 200-220MPa. On the other hand, maximum strain values were scattered for both types of specimens signaling a very important fact that the ability of weld materials against strain determines the failure of the specimens. When zoomed in into region B another important fact became clearly visible. Although some samples (independent from the process parameters) have high ultimate stress values their maximum strain values were below the base material which decreases the reliability of such specimens under operating conditions. From this perspective whole experiment set was divided into three categories:

Group A: "Low strain" samples that can occasionally give high stress values (WNZ Failed)

Group B: "Moderate strain" samples whose ε_{max} was below base material

Group C: "High strain samples" whose ε_{max} was above base material.

When the tensile test results of base material and un-aged FSW specimens observed it was clear that there is a larger yielding portion of the un-aged FSW specimens compared to base material. This distinction is clear especially in Group B and C specimens where relatively large strain values are achieved and most failures happen around HAZ region. In Fig. 5.1 the tensile test results of base material, un-aged FSW and aged FSW specimen taken from plate No. 26 can be seen. Mechanical properties for the two specimens are as follows:

Table 5. 1: Mechanical Properties of Base Material-26, Un-Aged FSW-26 and Aged FSW-26.

	UTS [MPa]	Yield Stress [MPa]	Max. Strain [%]
Base 26	304	285	8,58
FSW 26 Un-Aged	228	143	9,54
FSW 26 Aged	272,7	243,6	2,1

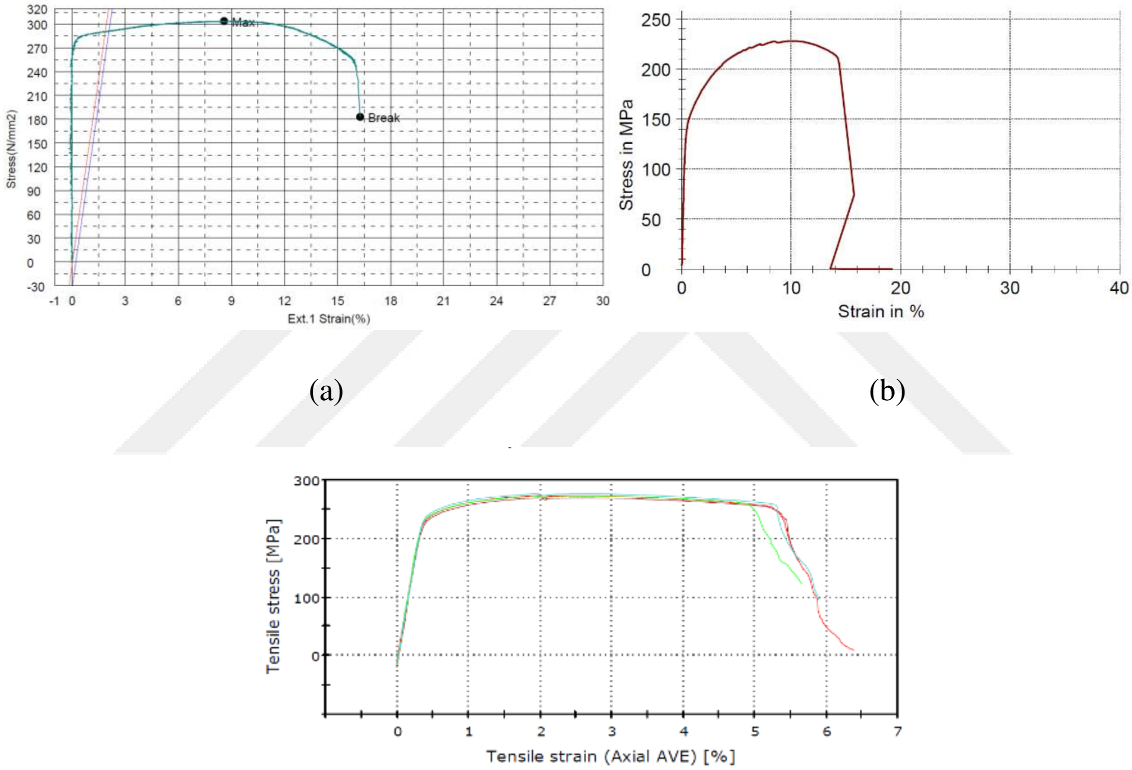

(a) (b)

(c)

Figure 5. 1: (a) Base Materal-26, (b) Un-Aged FSW-26 and (c) Aged FSW-26.

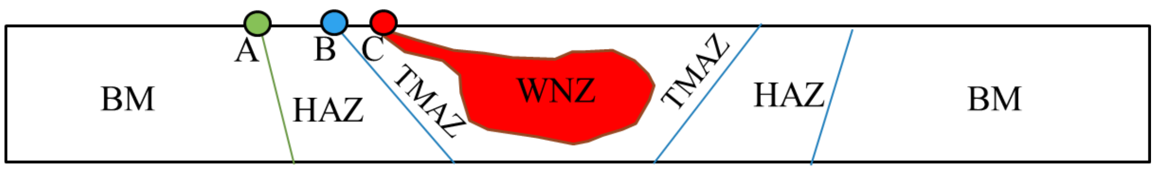

Figure 5. 2: Different Microstructural Zones and Interfaces.

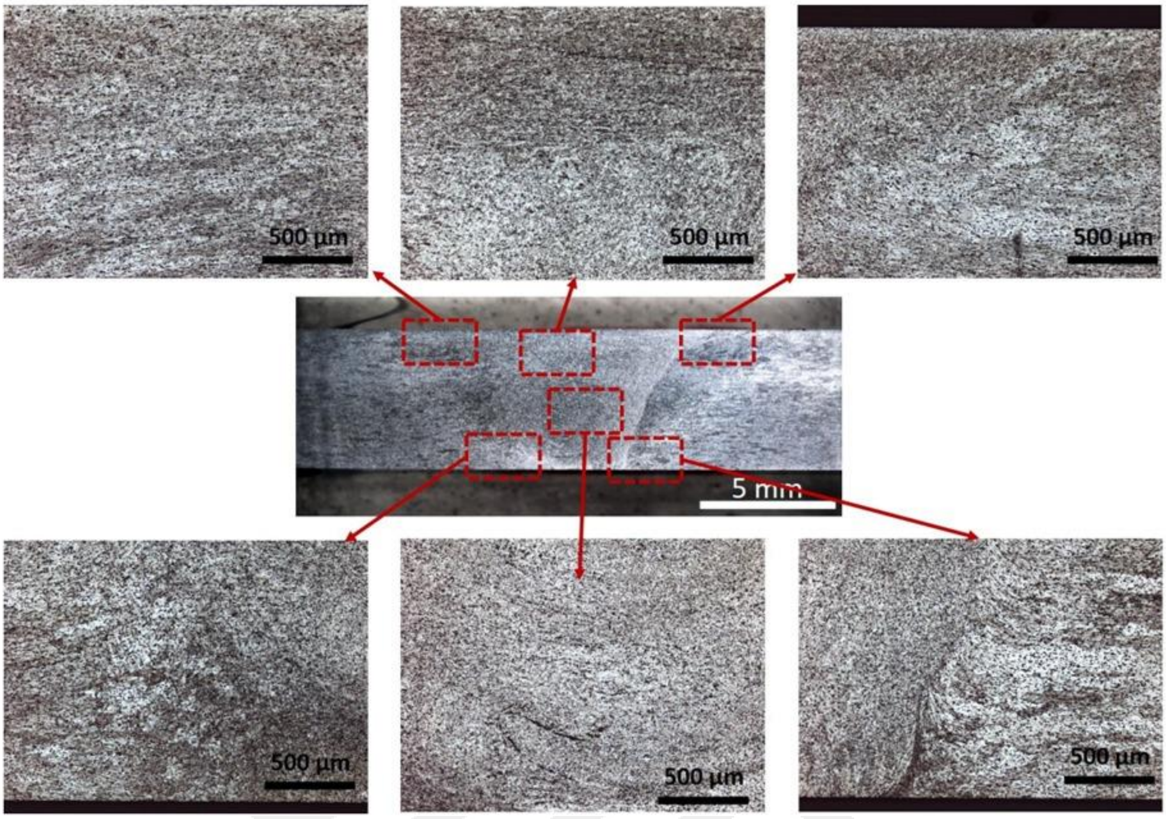

Figure 5. 3: Metallography Images of Un-Aged FSW-26 Specimens.

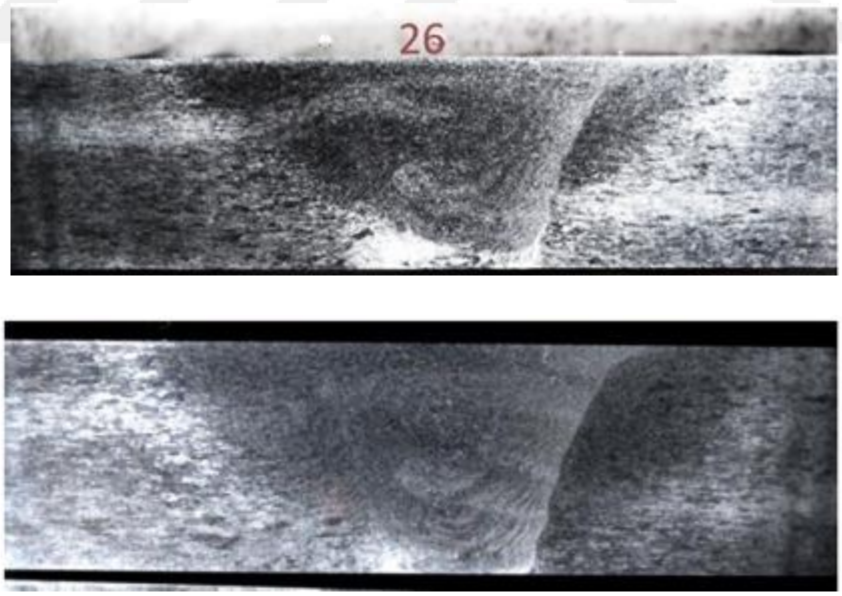

Figure 5. 4: Stereo Microscope Image of the Weld Zone for FSW-26 Un-Aged and Aged (respectively).

Base material distribution inside (white colored regions) different welding zones is shown in Fig. 5.4. Metallographic analysis suggested that the overall performance of welding zone is dependent on final base material distribution and shape of TMAZ-HAZ region.

Irregularities occurring during FSW process on zone interfaces may play an important role in failure. Such irregularities in the interfaces seems to be disappeared when samples are subjected to artificial aging conditions as it can be seen in Fig. 5.4.

In aluminum two main factors increase the strength and hardness of the material: precipitates and fine grain structure. Since base material is Al6061 in T6 condition, it is precipitation hardened by Al-Mg-Si particles [Chen et. al., 2020], thus the yield strength and UTS are close to each other. However, in FSW operation the HAZ region experiences temperatures around 500-550º C, where the melting point of Al6061 is around 650º C. Due to this heating effect the HAZ region softens and precipitates inside this region dissolves [Liu et. al., 2021], thus resulting in a softer material which yields earlier, and strains more compared to the base material. Ultimate strength of the material decreases as well.

TMAZ and weld nugget zone (WNZ) has fine grain structure due to mechanical deformation caused by the tool pin. Due to finer grain structure in specimen Groups B and C, failures are observed in HAZ region since TMAZ and WNZ are stronger. When failures are seen in TMAZ and WNZ region as it is usually the case in Group A type specimens, the failure is more brittle and strain levels are smaller.

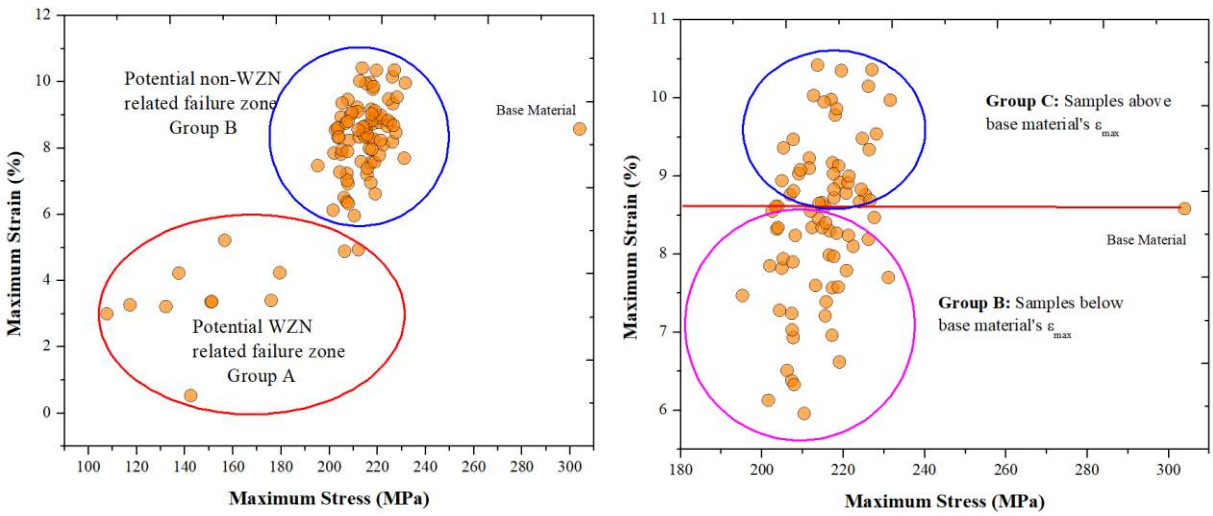

Figure 5. 5: Un-Aged Tensile Test Specimens Strain vs. UTS.

After the evaluation of un-aged specimens, aged specimens of the same test samples were added into the discussion. Aged specimens resulted in much higher UTS values, and they produced more consistent results compared to un-aged specimens, as it can be seen from Fig

5.6. Also, their strain values were dropped, however due to the increased reliability of the YS and UTS values, disadvantages of lowered strain values can be mitigated.

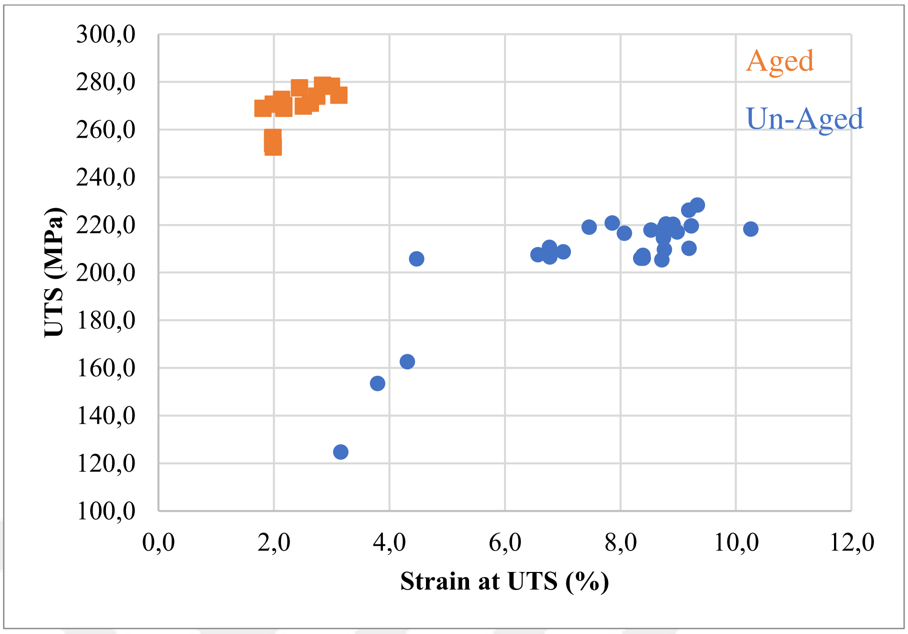

Figure 5. 6: Aged and Un-Aged Specimens - UTS vs. Strain Graph.

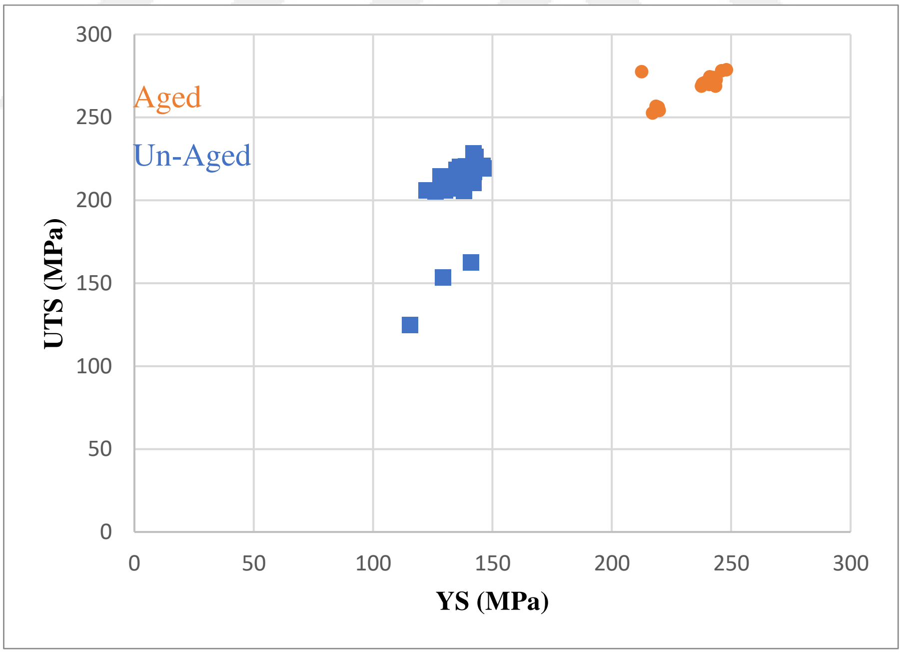

Figure 5. 7: Aged and Un-Aged Specimens - UTS vs. YS Graph.

Al6061-T6 is a precipitation-hardened aluminum alloy and its major alloying elements are Mg and Si. Al-Mg-Si precipitates increase the mechanical properties of Al6061 such as strength and hardness. However, these precipitates dissolve in aluminum matrix between 450 to 590ºC [Liu et. al., 2021]. During FSW process these temperatures are experienced throughout NZ, TMAZ and HAZ resulting in dissolution of precipitates, causing the material to become softer.

These precipitates can be regenerated via natural or artificial aging [Chen et. al., 2020]. Due to this reason, half of the tensile test and metallography samples cut out from Al6061-T6 plates were artificially aged to observe precipitation effects. Half of the tensile test specimens taken out of the friction stir welded plates were artificially aged at 180ºC for 8 hours.

In figure 5.6 the stress vs. strain graph of all specimens, aged and un-aged specimens taken from friction stir welded plates, can be seen. It is observed that un-aged specimens, which are taken out of the welded plates directly via water jet cutter, are much more dispersed compared to aged specimen results. Un-aged specimens show varying ductile properties as strain values range from 3.2% to 10.3%. Most un-aged specimens have high ductility as Group C specimens even exceed the strain values of base material. However, the strength of these specimens are low since most of them have UTS values that are lower than 220 MPa, and the highest UTS value measured is 228 MPa.

The aged specimens on the other hand are much more clustered and have consistent values. Their ductility is decreased as their strain values are around 2.5%. However, the formation of precipitates after the artificial aging process increases hardness and strength of the material, which is a more desirable outcome of the FSW process. It is also observed that the specimens' strength is increased as highest UTS value achieved becomes 278 MPa. This is expected since dissolved Al-Mg-Si precipitates are reappeared due to artificial aging process.

The hardening effect of Al-Mg-Si particles can be observed from Fig. 5.7 as well. In un-aged parts the yield strength of the material is around 60% of UTS. This is the result of the absence of precipitates inside the aluminum matrix, resulting in material to elongate and plastically deform a considerable amount before reaching UTS. In aged parts however, the yield strength becomes around 88% of UTS which is almost the same behavior with the base material (Yield Stress: 276 MPa, UTS: 310 MPa). This is the result of the hardening effect created by the Al-Mg-Si precipitates forming after the artificial aging process.

Table 5. 2: Overall Results for Un-Aged and Aged Al6061-T6 Samples.

#	RS	WS	DF	UTS (MPa)		Yield Stress (MPa)		Strain at UTS (%)	
				Unaged	Aged	Unaged	Aged	Unaged	Aged
1	-1	-1	-1	206,1	249,9	130,0	215,9	8,4	2,8
2	-1	-1	0	210,2	255,1	130,0	220,2	9,2	2,4
3	-1	-1	1	205,4	252,1	126,0	214,1	8,7	1,9
4	-1	0	-1	205,8	260,7	138,0	225,3	4,5	2,9
5	-1	0	0	220,3	270,1	136,3	231,0	8,9	3,9
6	-1	0	1	216,6	271,2	138,8	238,9	8,1	2,7
7	-1	1	-1	124,8	169,2	115,4	155,1	3,2	0,6
8	-1	1	0	153,6	219,5	129,2	210,0	3,8	0,6
9	-1	1	1	162,7	243,8	141,0	237,3	4,3	0,8
10	0	-1	-1	209,8	258,8	137,9	222,6	8,8	2,0
11	0	-1	0	207,6	256,2	136,3	219,4	6,6	2,0
12	0	-1	1	207,3	254,6	134,2	219,3	8,4	2,0
13	0	0	-1	217,1	271,2	142,3	239,3	9,0	2,6
14	0	0	0	219,3	274,1	146,2	242,3	8,8	2,7
15	0	0	1	206,6	269,0	137,9	243,4	6,8	1,8
16	0	1	-1	219,7	274,5	138,9	241,0	9,2	3,1
17	0	1	0	220,9	278,3	145,7	246,0	7,9	3,0
18	0	1	1	218,4	278,7	134,9	248,0	10,3	2,8
19	1	-1	-1	210,6	256,8	141,9	218,5	6,8	2,0
20	1	-1	0	208,9	254,2	136,6	219,8	7,0	2,0
21	1	-1	1	206,1	252,7	122,3	217,0	8,4	2,0
22	1	0	-1	217,9	270,3	139,8	237,9	8,5	2,2
23	1	0	0	220,5	270,7	138,9	238,3	8,8	2,0
24	1	0	1	214,5	268,9	128,3	237,4	8,7	2,2
25	1	1	-1	219,1	277,6	140,4	212,4	7,5	2,4
26	1	1	0	226,2	272,7	142,9	243,6	9,2	2,1
27	1	1	1	228,4	269,9	142,1	240,8	9,3	2,5
BM	-	-	-	304		285		9,7	

5.2 Effect of Process Parameters with Analysis of Variance Method

Analysis of variance (ANOVA) is a statistical analysis tool that compares the variations in the means of subgroups in a data set. It is used to determine the influence of independent variables on dependent variables or responses in a regression problem. It can be used to describe and make sense of the relations that independent variables of a process have with the desired outcomes.

FSW process is a complex method that utilizes more than one independent variable that have significant effect, which are also interacting with each other while affecting the outcome. Due to the complex nature of the FSW process, it is suitable to utilize a statistical analysis tool such as ANOVA to analyze the effects of independent process parameters on the process responses.

Independent variables used for this analysis are; Rotational Speed (RPM), Advancing Speed (mm/min) and Down Force (N). To examine the effects of these variables, UTS and Yield Stress of aged and un-aged specimens are used. To implement the ANOVA on the data set, Stat-Ease 360 program was used.

Four fundamental properties determined via mechanical testing which are i) un-aged UTS, ii) un-aged Yield Stress, iii) aged UTS and iv) aged Yield Stress were considered as responses. ANOVA analysis is employed to create surrogate models taking process parameters as variables and mechanical testing results as responses.

5.2.1 Effect of process parameters on Un-Aged Specimens – UTS

A p-value is a measurement used to validate the hypothesis in comparison with the observed data. A lower p-value signals greater statistical significance. Generally, a value lower than 0,05 is considered important. In this research limit for p-value significance is taken as 0,05.

R^2 is statistical measurement to reflect the quality of the model by indicating how much of a variance in the dependent variable can be explained by a change in the independent variables. A higher R^2 value is preferred since it shows the reliability of the projected model for explaining the behavior of the dependent variables.

When analyzing the dependent variable, UTS, for un-aged specimens the model type was suggested by the statistical analysis program as ‘Linear’. The reason for this is that a linear model best represents the underlying data for the un-aged UTS values, according to the p-value and R^2 valuations as it can be seen from Table 5.3.

Response 1: UTS

Table 5. 3: Fit Summary for Un-Aged UTS.

Source	Sequential p-value	Lack of Fit p-value	Adjusted R^2	Predicted R^2	
Linear	**< 0.0001**		**0,6526**	**0,5691**	**Suggested**
2FI	0,3935		0,6555	0,4983	
Quadratic	0,1637		0,7062	0,4600	
Cubic	0,4464		0,7217	-0,3930	**Aliased**

According to the ANOVA Linear Model in Table 5.4 the most significant independent variable when evaluating the un-aged UTS values is the welding speed, which has the lowest p-value. Whereas down force appeared insignificant in un-aged UTS.

Table 5. 4: ANOVA for Linear Model Response: UTS.

Source	Sum of Squares	Df	Mean Square	F-value	p-value	
Model	766,31	3	255,44	15,40	< 0.0001	Significant
A-Rotational Speed	31,79	1	31,79	1,92	0,1815	
B-Welding Speed	627,99	1	627,99	37,86	< 0.0001	
C-Down Force	0,5323	1	0,5323	0,0321	0,8596	
Residual	331,76	20	16,59			
Cor Total	1098,07	23				

Table 5. 5: Final Equation in Terms of Coded Factors.

	Intercept	A	B	C
UTS	214,96	1,52	6,73	-0,18

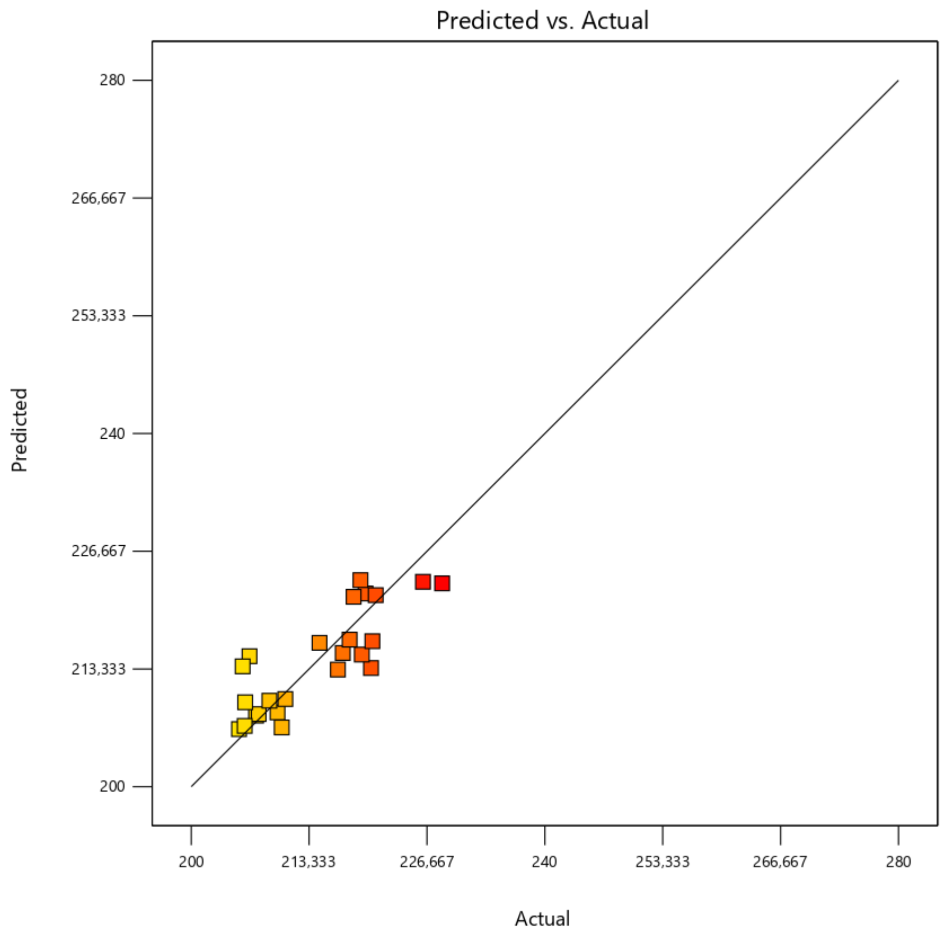

Figure 5. 8: Predicted vs. Actual Values: Un-Aged UTS.

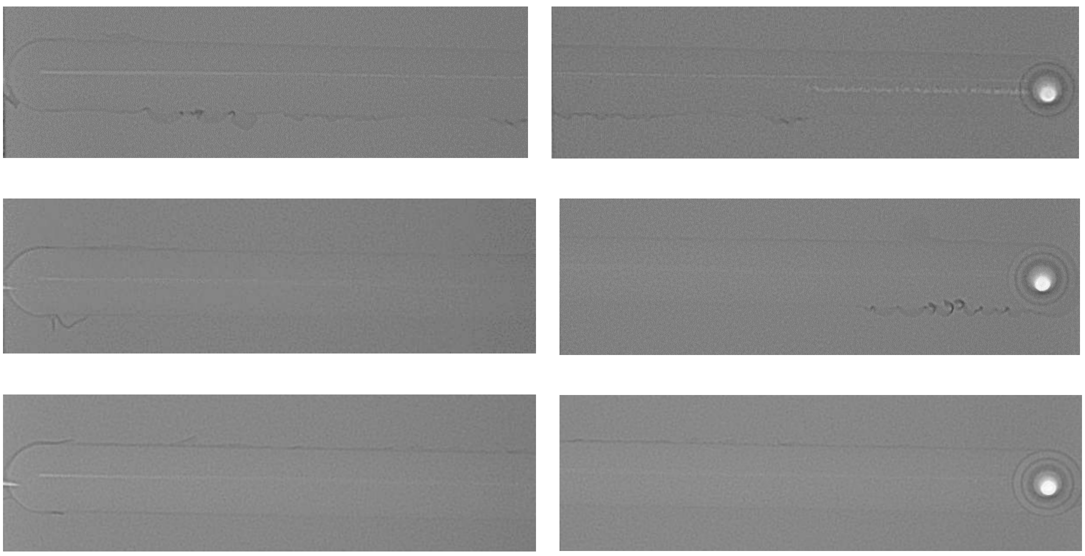

Figure 5. 9: Radiography Images of Samples 7-8-9 (respectively from top to bottom).

In Fig. 5.8, it can be seen that predicted values and actual values are close to each other as a result of a good regression model. Most of the sample points lay close to the 45-degree linear line as predicted and actual values match. Other data points are also very close to the linear line as the linear model created for un-aged UTS values works well. Samples 7-8-9 were discarded from the model because these samples had welding defects inside their weld zones which were detected during radiographical (Fig. 5.9) examination. These three samples are the only ones with welding defects, and they were creating disturbance in the model which was not due to the nature of the model or process and was not making any sensical contribution to the analysis. Therefore, excluding these three specimens from the analysis was best practice.

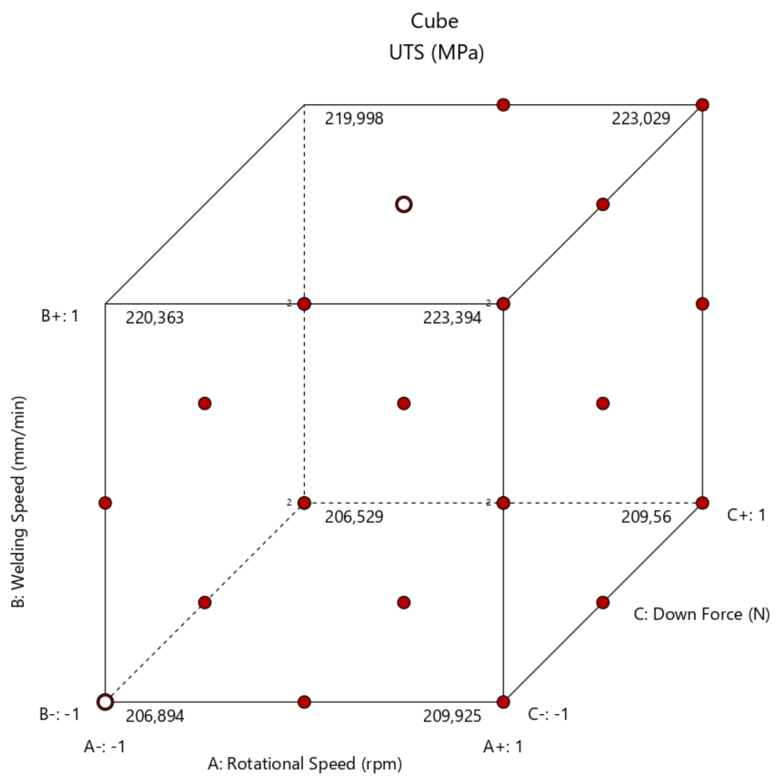

Figure 5. 10: Cube Plot of Data Points for Un-Aged UTS.

Fig. 5.10 shows the effects that process parameters have on UTS values with a three-dimensional cube graph. '-1' represents the minimum value of independent variable and '+1' represents the maximum value of the independent variable.

With increasing rotational speed, UTS values acquired increase. However, this effect is very insignificant as the UTS values change only about 1.5% with changing the rotational speed from minimum to maximum. This insignificance was also seen in the p-value of this variable which was 0,18.

Down force has even less effect on UTS value as virtually no change happens in UTS values with varying down force from minimum to maximum. P-value of down force in this linear model is 0,86, making it the least significant factor. This claim is evident in the observation.

Welding speed has the lowest p-value which is less than 0.0001 and it is seen as the most significant factor for un-aged specimens' UTS values. Increase in welding speed increases the UTS values of the specimens. This can be the result of lower heat input due to the fast-traveling rate of the FSW tool. High welding speed does not allow the weld piece to heat up too much, which otherwise would dissolve the Al-Mg-Si precipitates and soften the material.

5.2.2 Effect of process parameters on Un-Aged Specimens – Yield Stress

When analyzing the dependent variable, Yield Stress, for un-aged specimens the model type was suggested by the statistical analysis program as 'Quadratic' and 'Linear'. Quadratic type model was chosen based on its higher adjusted R^2 value.

Response 2: Yield Stress

Table 5. 6: Fit Summary for Un-Aged Yield Stress.

Source	Sequential p-value	Lack of Fit p-value	Adjusted R^2	Predicted R^2	
Linear	**0,0056**		**0,3784**	**0,2002**	**Suggested**
2FI	0,1208		0,4758	0,1423	
Quadratic	**0,0673**		**0,6117**	**0,1652**	**Suggested**
Cubic	0,2657		0,7054	-0,4691	**Aliased**

Based on the ANOVA model parameters in Table 5.7; welding speed and down force have significance in determining the outcome of un-aged yield stress. Additionally, the combination of rotational speed and down force have significant contribution to the result.

Table 5. 7: ANOVA for Quadratic Model Response: Un-Aged Yield Stress.

Source	Sum of Squares	df	Mean Square	F-value	p-value	
Model	633,39	9	70,38	5,03	0,0037	Significant

A-Rotational Speed	13,90	1	13,90	0,9928	0,3360	
B-Welding Speed	115,42	1	115,42	8,24	0,0123	
C-Down Force	67,93	1	67,93	4,85	0,0449	
AB	0,1433	1	0,1433	0,0102	0,9208	
AC	68,54	1	68,54	4,89	0,0441	
BC	63,12	1	63,12	4,51	0,0521	
A^2	58,05	1	58,05	4,14	0,0611	
B^2	23,49	1	23,49	1,68	0,2162	
C^2	56,83	1	56,83	4,06	0,0636	
Residual	196,06	14	14,00			
Cor Total	829,45	23				

Table 5. 8: Final Equation in Terms of Coded Factors.

	Intercept	**A**	**B**	**C**	**AB**	**AC**	**BC**	**A^2**	**B^2**	**C^2**
Yield Stress	143,02	1,20	3,45	-2,13	-0,16	-2,72	2,62	-3,53	-2,24	-3,26

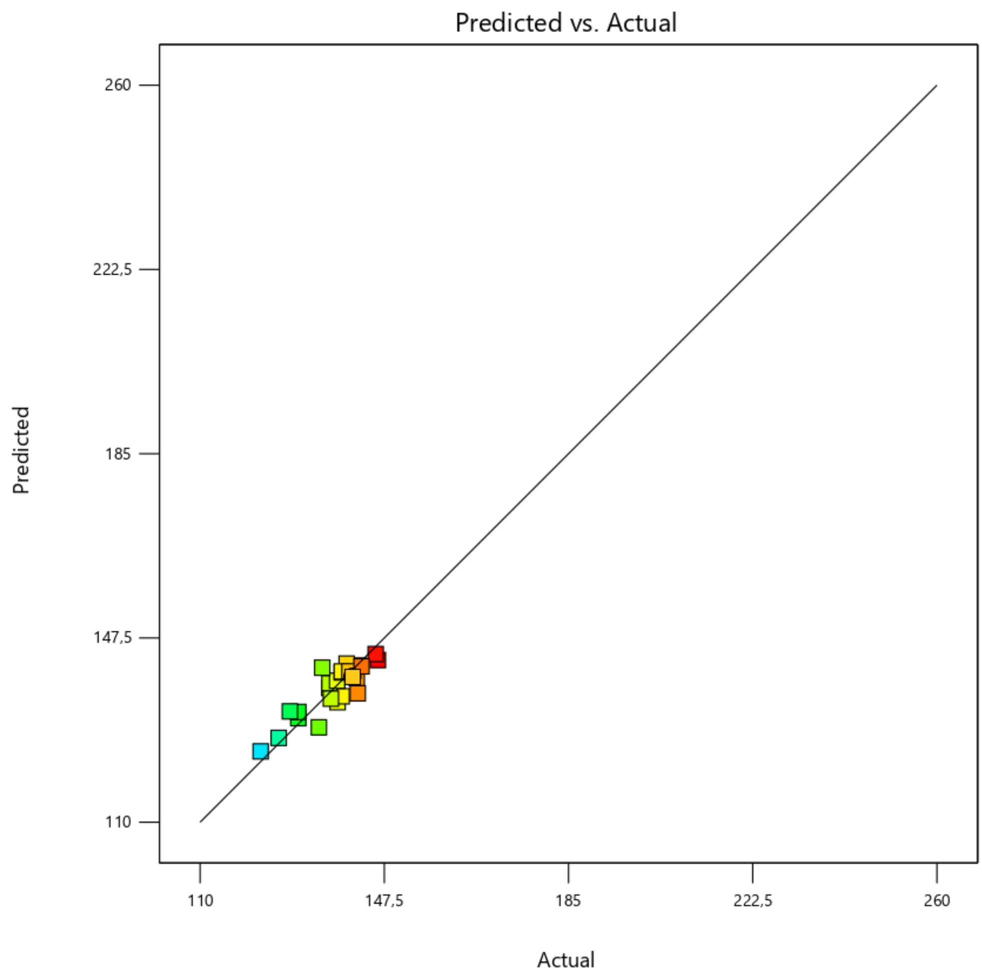

Figure 5. 11: Predicted vs. Actual Values: Un-Aged Yield Stress.

In Fig. 5.11 the predicted values by the model vs. actual values plot can be seen. In contrast to Fig. 5.8 for UTS values, yield stress predictions appear to be more accurate. However, this is due to the fact that observed yield stress values for un-aged specimens have less variance compared to other responses. This is the result of the failure mechanism that governs the un-aged specimens, especially at the initiation of yielding. Although different microstructures due to changing process parameters have been obtained, yielding mechanism in un-aged stir welded specimens do not get affected by the process parameters as much as other responses. Approximate average value of 130 MPa is a well-defined shear stress limit for AL6061-T6 samples. Hence it can be deducted that the observed yield stress in specimens is mostly due to shearing of base material dispersed in HAZ-TMAZ regions. Dispersion of base material in these regions can be seen in Fig. 5.12, where white colored regions contain base material.

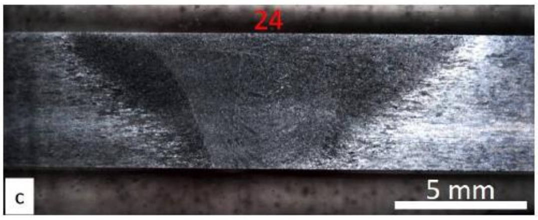

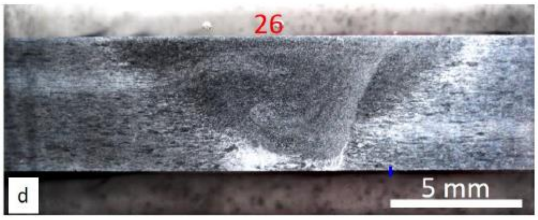

(a) (b)

Figure 5. 12: Stereo Microscope Images of Un-Aged Metallography Samples from (a) No. 24, (b) No. 26 Weld Plates

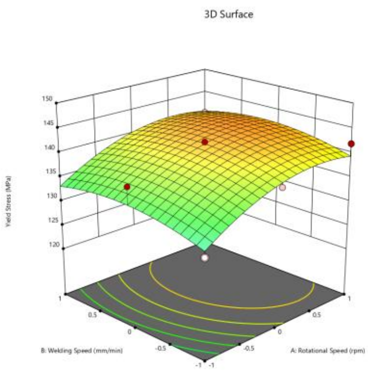

(a)

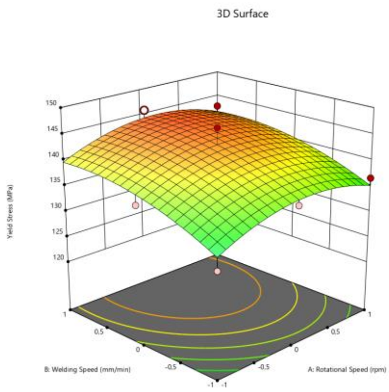

(b)

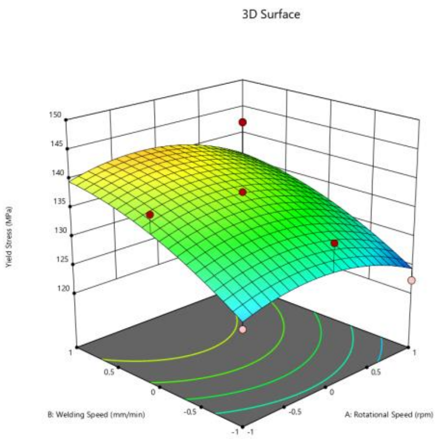

(c)

Figure 5. 13: 3D Surface Plot of the Model of Rotational Speed vs. Welding Speed vs. Yield Stress ((a)Down Force = -1, (b)Down Force = 0, (c) Down Force = 1).

Observed maximum yield stress value for un-aged specimens is approximately 146 MPa which can be seen in samples 14 and 17 in Table 5.2. In both of these samples rotational speed and down force are at mid-range values (0), which are 1400 RPM and 3500 N respectively. This result can also be interpreted from the 3D surface plots of the created model. In Fig. 5.13b, maximum yield stress predictions appear in mid-range rotational speed and down force values, while welding speed can be between the mid-range maximum value.

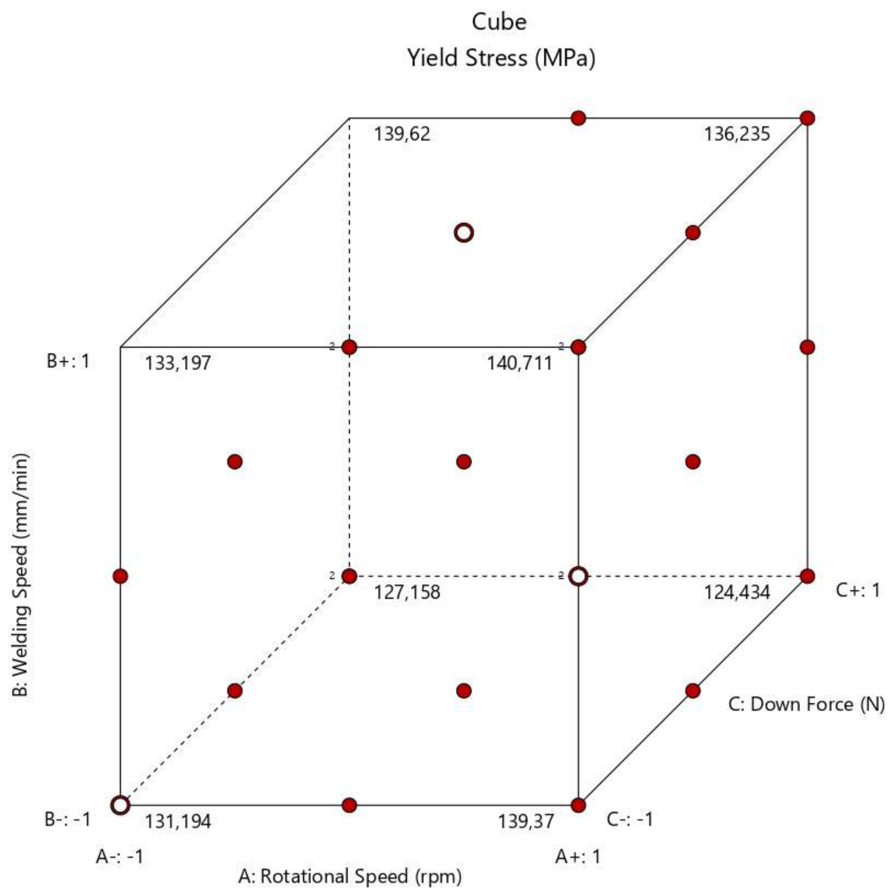

Figure 5. 14: Cube Plot of Data Points for Un-Aged Yield Stress.

5.2.3 Effect of process parameters on Aged Specimens – Yield Stress

When analyzing the third response, Aged-Yield Stress, model type was suggested as quadratic based on higher R^2 values as it can be seen in Table 5.9.

Response 3: Aged-Yield Stress

Table 5. 9: Fit Summary for Aged Yield Stress.

Source	**Sequential p-value**	**Lack of Fit p-value**	**Adjusted R^2**	**Predicted R^2**	
Linear	0,0008		0,4918	0,3331	

2FI	0,0832		0,5918	0,2375	
Quadratic	**0,0112**		**0,7699**	**0,5098**	**Suggested**
Cubic	0,5201		0,7654	-0,2371	**Aliased**

Based on the ANOVA model parameters Table 5.10; welding speed has the most significance in affecting aged yield stress response. It appears that down force also has significance due to its low p-value. Additionally, the combination of welding speed and down force have major contribution to the result. The square of the rotational speed term and square of the welding speed terms appear to affect the model significantly.

Table 5. 10: ANOVA for Quadratic Model Response: Aged-Yield Stress.

Source	**Sum of Squares**	**df**	**Mean Square**	**F-value**	**p-value**	
Model	2788,89	9	309,88	9,55	0,0001	significant
A-Rotational Speed	2,91	1	2,91	0,0898	0,7689	
B-Welding Speed	918,11	1	918,11	28,30	0,0001	
C-Down Force	186,16	1	186,16	5,74	0,0311	
AB	12,53	1	12,53	0,3862	0,5443	
AC	0,4197	1	0,4197	0,0129	0,9110	
BC	225,93	1	225,93	6,97	0,0194	
A^2	209,89	1	209,89	6,47	0,0234	
B^2	362,68	1	362,68	11,18	0,0048	
C^2	50,93	1	50,93	1,57	0,2307	
Residual	454,13	14	32,44			
Cor Total	3243,01	23				

Table 5. 11: Final Equation in Terms of Coded Factors.

	Intercept	**A**	**B**	**C**	**AB**	**AC**	**BC**	**A^2**	**B^2**	**C^2**

Aged-Yield Stress	243,62	0,54	9,73	3,52	-1,54	-0,21	4,95	-6,71	-8,82	-3,09

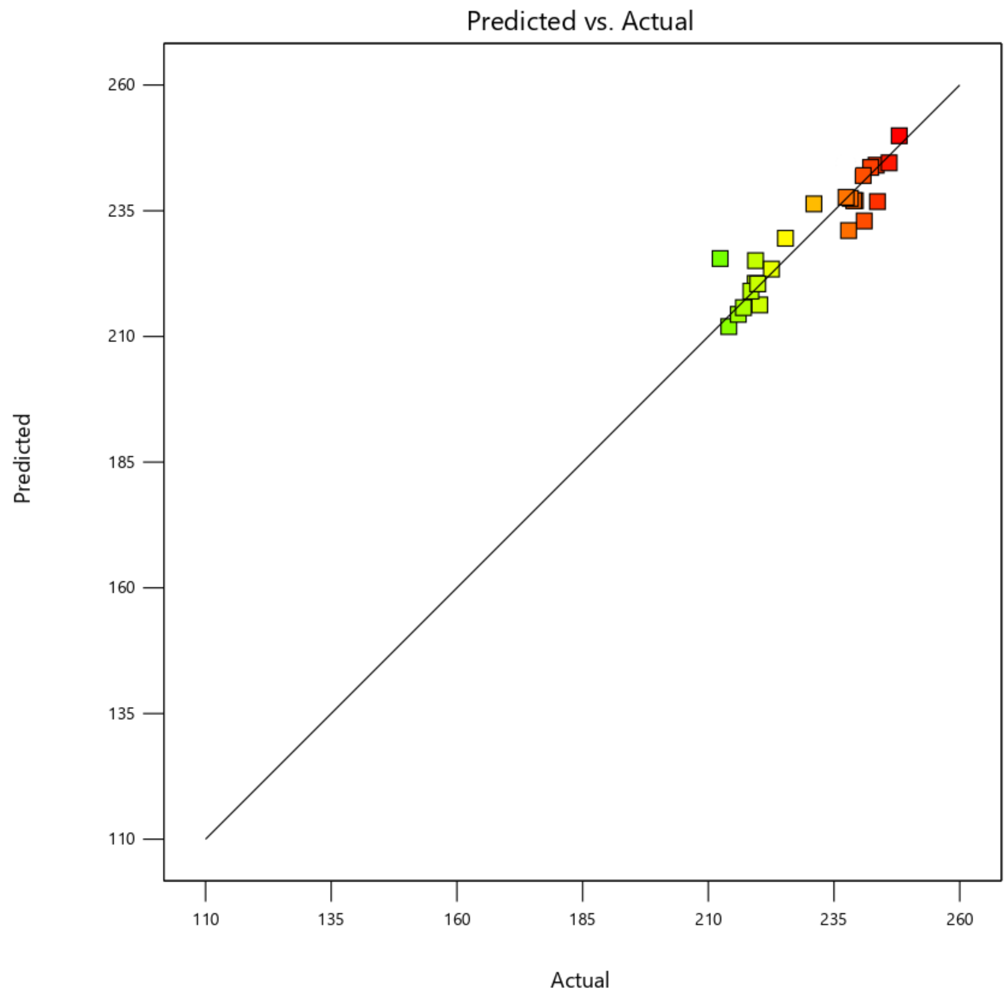

Figure 5. 15: Predicted vs. Actual Values: Aged Yield Stress.

In Fig. 5.15 the predicted values by the model vs. actual values plot for aged-yield stress values can be seen. Observed yield stress values appear to be almost doubled compared to un-aged yield stress values. This feature was also evident in Fig. 5.7 as after the aging process specimens' yield stress values came close to their UTS values due to precipitation hardening effects.

Aged-yield stress predictions appear to be significantly accurate since most points lay on the 45-degree linear line. There is more variance in the observed data, compared to un-aged yield stress values, which is due to the change in failure mechanism of the specimens after the aging process. The change in microstructure after the aging process can be observed in Fig. 5.16b compared to Fig. 5.12b. Base material dispersion among HAZ-TMAZ regions has disappeared significantly. Instead of the base material, precipitates appear in these zones which are shaded with black as they increase the hardness and strength of the specimens.

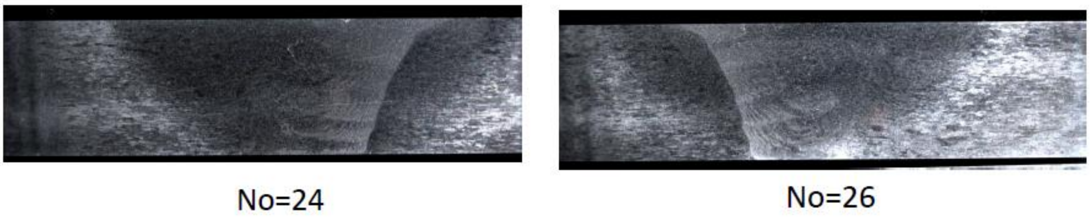

(a) (b)

Figure 5. 16: Stereo Microscope Images of Aged Metallography Samples from (a) No. 24 and (b) No. 26 Weld Plates.

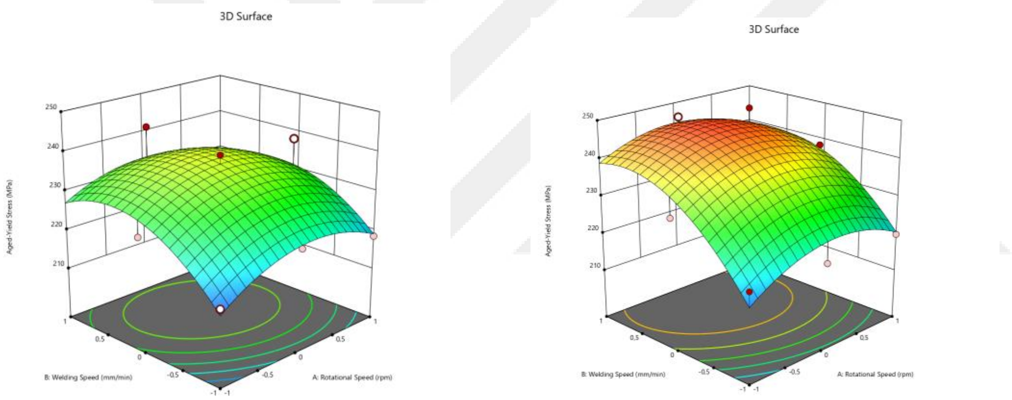

(a) (b)

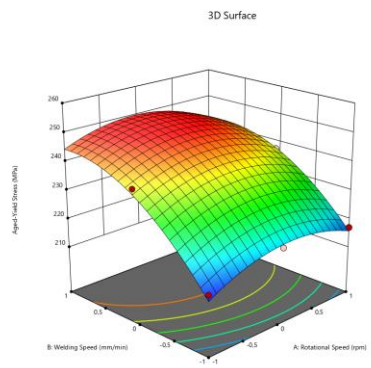

(c)

Figure 5. 17: 3D Surface Plot of the Model of Rotational Speed vs. Welding Speed vs. Aged-Yield Stress ((a) Down Force = -1, (b) Down Force = 0 and (c) Down Force = 1).

Observed maximum yield stress values for aged specimens is approximately 248 MPa which can be seen in sample 18 in Table 5.2. At this sample rotational speed is mid-range (0), welding speed is maximum (1) and down force is maximum (1), which are 1400 RPM, 700 mm/min and 4000 N. In Fig. 5.17c maximum yield stress predicted by the model occurs at the region where rotational speed is at its mid-range values and both down force and welding speed are at their maximum, which is in good agreement with the observation.

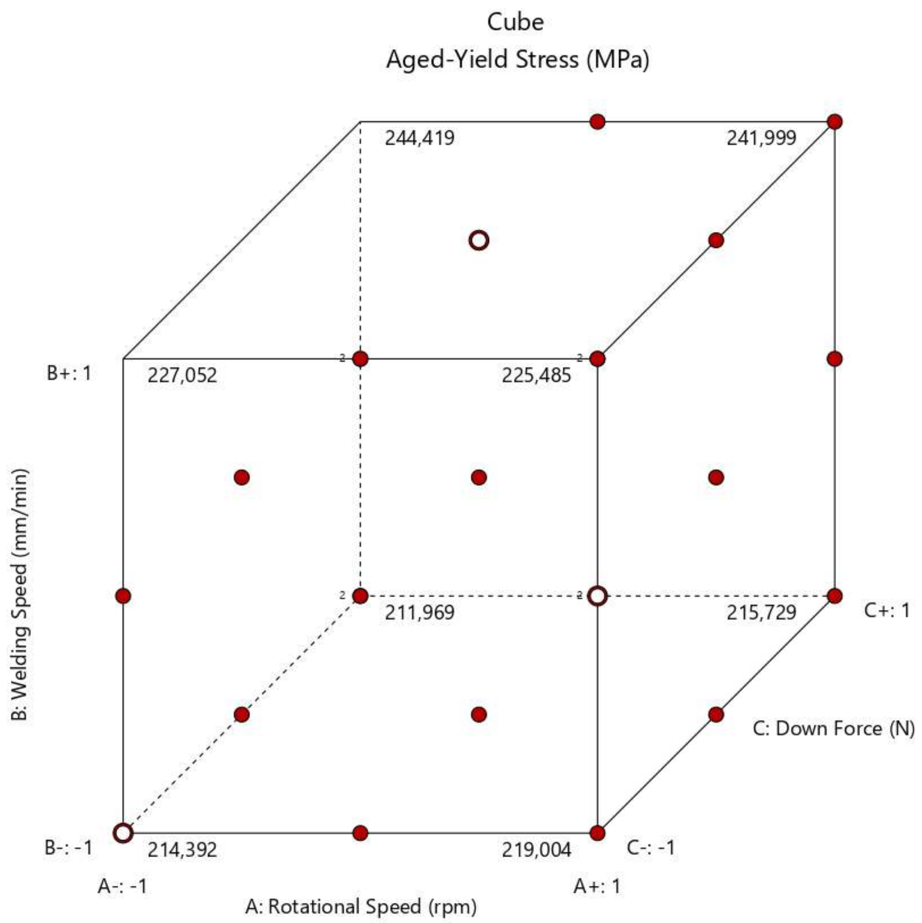

Figure 5. 18: Cube Plot of Data Points for Aged Yield Stress.

5.2.4 Effect of process parameters on Aged Specimens – UTS

Last response analyzed is UTS values of the artificially aged specimens. Model type is chosen as quadratic since R^2 values are significantly high signaling a very good model as it can be seen in Table 5.12.

Response 4: Aged-UTS

Table 5. 12: Fit Summary for Aged Yield Stress.

Source	Sequential p-value	Lack of Fit p-value	Adjusted R^2	Predicted R^2	
Linear	< 0.0001		0,8044	0,7537	
2FI	0,0534		0,8516	0,7671	
Quadratic	**0,0007**		**0,9446**	**0,8890**	**Suggested**
Cubic	0,0803		0,9728	0,8921	**Aliased**

Based on the ANOVA model parameters Table 5.13; welding speed has the most significance in affecting aged UTS response. It appears that the combination of rotational speed and down force have major effect as well. Additionally, square of rotational speed and square of welding speed terms are significant.

Table 5. 13: ANOVA for Quadratic Model Response: Aged-UTS.

Source	Sum of Squares	df	Mean Square	F-value	p-value	
Model	1972,81	9	219,20	44,54	< 0.0001	significant
A-Rotational Speed	6,94	1	6,94	1,41	0,2548	
B-Welding Speed	976,84	1	976,84	198,49	< 0.0001	
C-Down Force	1,34	1	1,34	0,2714	0,6106	
AB	1,22	1	1,22	0,2475	0,6266	
AC	73,09	1	73,09	14,85	0,0018	
BC	7,23	1	7,23	1,47	0,2455	
A^2	49,08	1	49,08	9,97	0,0070	
B^2	119,15	1	119,15	24,21	0,0002	
C^2	13,78	1	13,78	2,80	0,1164	
Residual	68,90	14	4,92			
Cor Total	2041,71	23				

Table 5. 14: Final Equation in Terms of Coded Factors.

	Intercept	A	B	C	AB	AC	BC	A^2	B^2	C^2
Aged-UTS	272,82	0,84	10,04	0,29	-0,48	-2,81	0,88	-3,24	-5,05	-1,61

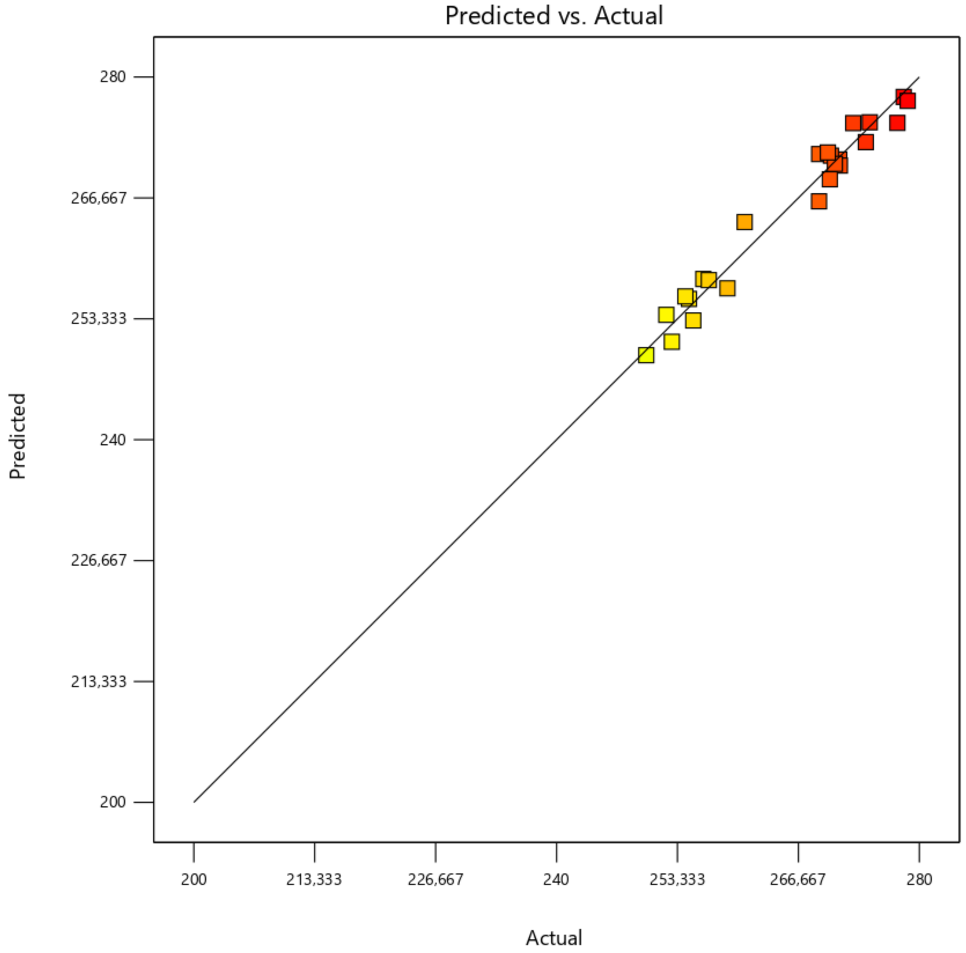

Figure 5. 19: Predicted vs. Actual Values: Aged UTS.

In Fig. 5.19 the predicted values by the model vs. actual values plot for aged-UTS values can be seen. Observed aged-UTS values appear to be increased by approximately 25% compared to un-aged UTS values. UTS values as high as 278 MPa are achieved in this data set which is approximately 90% of the base material UTS. This is a very high efficiency in terms of strength for any permanent joining method.

Aged-UTS predictions are accurate since most of the data points on Fig. 5.19 lay on the 45-degree line. It appears there are two groups clustered having means of 254 and 271 MPa.

Group that has the mean of 254 MPa consist of samples 1-2-3-10-11-12-19-20-21. All these samples have welding speed parameter at its lowest setting (-1). The other group, which consists of rest of the samples, has the mean of 271 MPa and have welding speed parameter as either (0) or (1). This is in good agreement with the claim that due to low welding speed there is more heat input to the weld zone and Al-Mg-Si particles disappear significantly. Due to this heat effect the UTS values of the samples with low welding speed is observed to be less than the other samples.

Same effect on UTS values can also be seen in un-aged UTS values in Table 5.2 and a similar clustering of two groups can be observed in Fig. 5.8. Samples 1-2-3-10-11-12-19-20-21 have a mean of 207 MPa, and rest of the samples have a mean of 217 MPa. This observation emphasizes the significance of the welding speed in FSW process and on its responses.

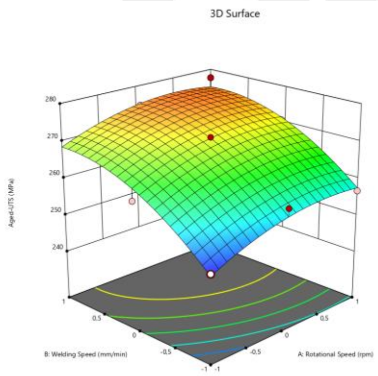

(a)

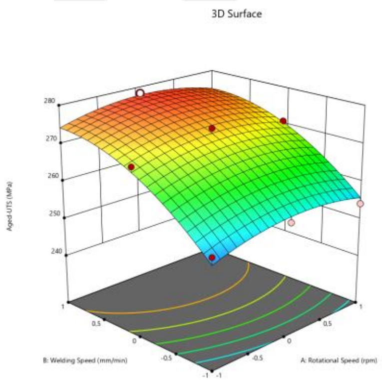

(b)

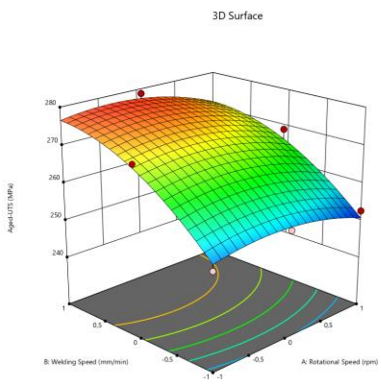

(c)

Figure 5. 20: 3D Surface Plot of the Model of Rotational Speed vs. Welding Speed vs. Aged-UTS ((a) Down Force = -1, (b) Down Force = 0 and (c) Down Force = 1).

Observed maximum UTS value for aged specimens is approximately 278 MPa which can be seen in samples 17 an 18 in Table 5.1.1. At these sample rotational speed is mid-range (0), welding speed is maximum (1) and down force is mid-range (0) and maximum (1), which are 1400 RPM, 700 mm/min, 3500 N and 4000 N, respectively. In Fig. 5.20b and Fig. 5.20c, maximum UTS predicted by the model occurs at the regions where rotational speed is at its mid-range values and welding speed is at its maximum value. Additionally, both mid-range and maximum down force values result in maximum UTS predictions, which is in good agreement with the observation.

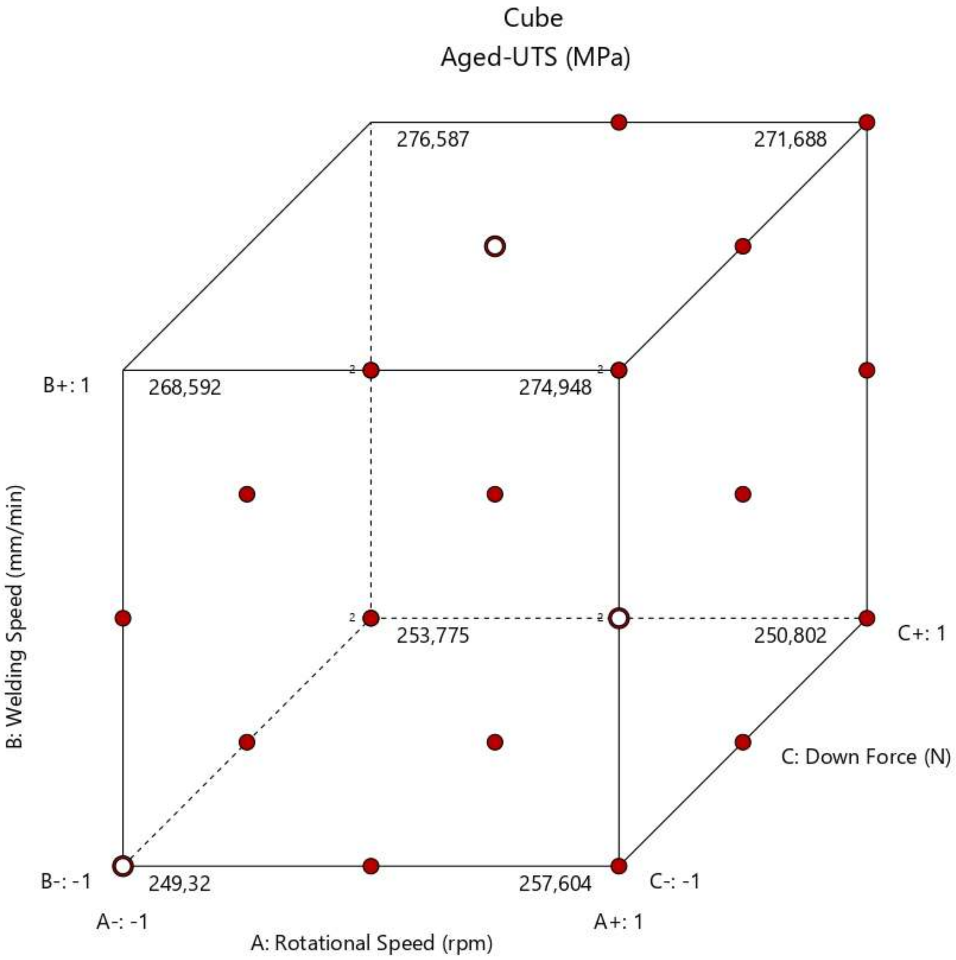

Figure 5. 21: Cube Plot of Data Points for Aged UTS.

Table 5. 15: Final Equations of All Responses in Terms of Coded Factors.

	R^2	**Intercept**	**A**	**B**	**C**	**AB**	**AC**	**BC**	A^2	B^2	C^2
Un-Aged UTS		214,96	1,52	6,73	-0,1824						
Un-Aged Yield Stress		143,02	1,20	3,45	-2,13	-0,16	-2,72	2,62	-3,53	-2,24	-3,26
Aged Yield Stress		243,62	0,54	9,73	3,52	-1,54	-0,21	4,95	-6,71	-8,82	-3,09
Aged UTS		272,82	0,84	10,04	0,29	-0,48	-2,81	0,88	-3,24	-5,05	-1,61

A = Rotational Speed

B = Welding Speed

C = Down Force

5.3 Optimization

Using the produced model, desired outcomes can be optimized. Maximizing the yield stress and ultimate tensile stress for aged specimens is the most desirable outcome for a FSW process in terms of joining strength.

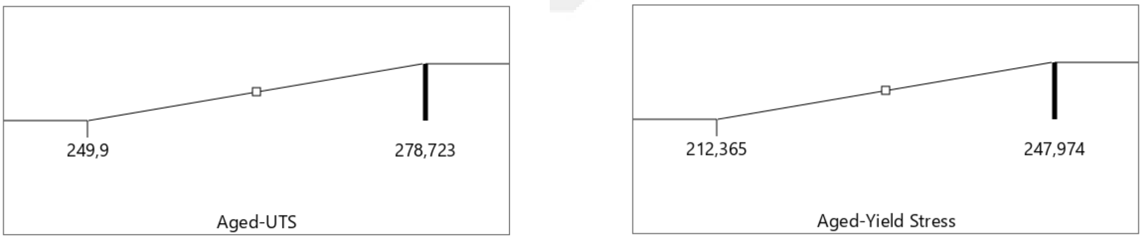

(a) (b)

Figure 5. 22: Criteria for Optimization.

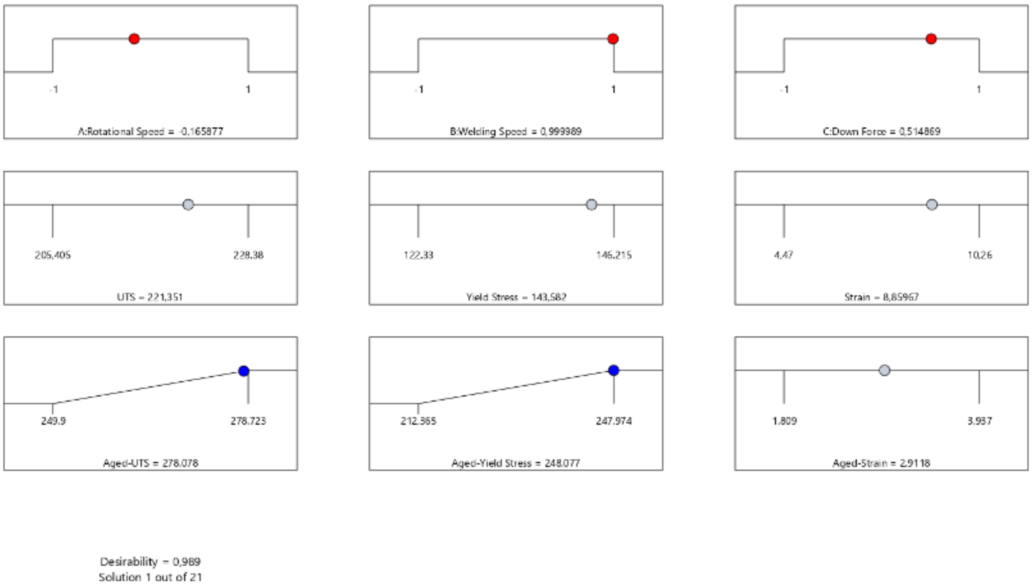

Figure 5. 23: Solution Values.

In order to get to the desired criteria, 21 possible solutions are produced which are very similar to each other in terms of process parameter values. As it can be seen from Fig. 5.23 ‘Solution 1’ is chosen with a desirability of 0,989, which is a very significant value for a regression model. In good agreement with the discussion presented in subsection 5.2.4, the solution produces; rotational speed to be very close to mid-range, welding speed to be maximum and down force to be between mid-range and maximum.

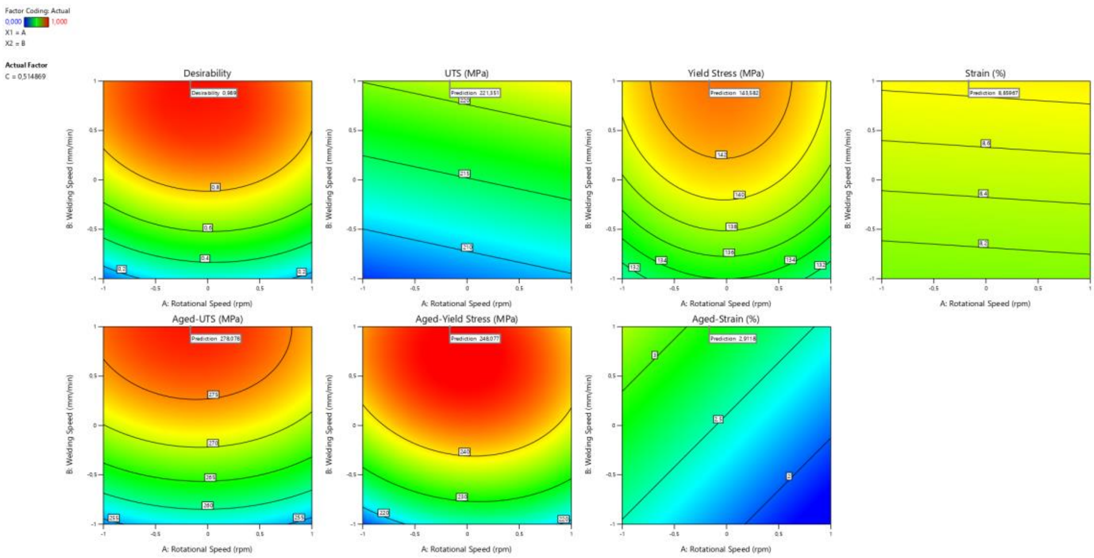

Figure 5. 24: Solution Contour Graph.

Optimized Solution:

- Rotational Speed = 1317 RPM
- Welding Speed = 700 mm/min
- Down Force = 3757 N

5.4 Model Verification Tests

After generating optimized solution for maximizing aged yield stress and aged ultimate tensile stress, these parameters were used to weld two pair of test plates (TP). Both plates were welded with optimized solution parameters and tensile test specimens were cut according to ASTM E8. Half of the samples were un-aged and half of the samples were artificially aged for 8 hours at 180°C. The results can be seen in Table 5.16.

Table 5. 16: Model Verification Test Results.

	Aged UTS [MPa]		**Aged YS [MPa]**		**Un-Aged UTS [MPa]**		**Un-Aged YS [MPa]**	
	Test Plate (TP) 1	TP 2	TP 1	TP 2	TP 1	TP 2	TP 1	TP 2
Predicted	278		248		221		143	
Observed	272	277	247	254	215	222	149	151
Error	2,1%	0,3%	0,4%	2,4%	2,7%	0,4%	4,1%	5,5%

As it can be seen from Table 5.16, model predictions are very accurate. Aged YS and Aged UTS predictions are very close to observed values with less than 2,5% error, since these models have the highest R^2 as well. Un-aged values are extremely close to the observed values as well. Un-aged YS model has the lowest R^2 value but even those predictions are less than 6% error margin. Overall, generated ANOVA model works very accurately and successfully.

CHAPTER 6:
CONCLUSION

6.1 Final Remarks

In this study, the effects of process parameters which are: Rotational Speed, Welding Speed and Down Force were investigated on mechanical strength of Al 6061-T6 alloy once it is joined with FSW method. Set of experiments designed and analyzed with Analysis of Variance technique to better understand the interrelations of process parameters and complex dynamics of the process. FSW plates were prepared and joined according to the design of experiments set and post welding examinations conducted. Half the samples taken out from the joined plates were artificially aged and half of them were examined without aging, resulting in 54 different experiment points. The effects of process parameters were determined on both heat treatment conditions. This approach also intensified the importance of post-weld heat treatment of FSW process and the precipitation hardening effects of Al6061 alloy. A valuable regression model is created from the experiment set. Both the effects of process parameters are clearly observed and predicted as well as fracture mechanisms are better understood via the metallographic examinations which contributed to form a better model and approach. Welding speed is found to be the most significant parameter amongst the three process parameters. Artificial aging after the welding operation is proved to be highly beneficial in terms of mechanical strength of the joint line. Optimized solutions are obtained from the data set with good agreement with the observed data. For further improvements, the effect of pin shape on microstructural distribution can be studied. This could lead to a better understanding of the failure mechanism inside and to better engineer the strain levels for failure.

6.2 Future Works

For future work, seam welding of a pressure vessel made of Al6061-T6 will be joined with FSW. Different parameter values will be utilized for the welding process and UTS and YS values higher than conventional fusion welding values will be aimed to increase the weld line strength. This method will enable producing lighter and stronger pressure vessels, also it will remove the limitations regarding the diameter of tubular body.

BIBLIOGRAPHY

[Mishra et. al., 2014] Mishra R.S., De P.S., and Kumar N. (2014) Friction Stir Welding and Processing. *Springer.*

[Langari et. al., 2016] J. Langari, F. Kolahan, and K. Aliakbari (2016) Effect of Tool Speed on Axial Force, Mechanical Properties and Weld Morphology of Friction Stir Welded Joints of Al7075-T651. *International Journal of Engineering.*

[Rambabu et. al., 2015] G. Rambabu, D. Balaji Naik, C.H. Venkata Rao, K. Srinivasa Rao, and G. Madhusudan Reddy (2015) Optimization of Friction Stir Welding Parameters for Improved Corrosion resistance of AA2219 Aluminum Alloy Joints.

[Cao et. al., 2005] G. Cao and S. Kou (2005) Friction Stir Welding of 2219 Aluminum: Behavior of Θ (Al_2Cu) Particles. *Welding Journal.*

[ISO, 2020] International Organization for Standardization (2020) Friction Stir Welding – Aluminum

[Fuiji et. al., 2006] Fuiji H., Cui L., Maeda M., and Nogi K. (2006) Effect of Tool Shape on Mechanical Properties and Microstructure of Friction Stir Welded Aluminum Alloys. *Materials Science and Engineering.*

[Kallee et. al., 2001] Kallee S. W., Nicholas E. D., and Thomas W. M. (2001) Friction Stir Welding – Inventions, Innovations and Applications.

[Boonma et. al., 2015] Boonma J., Khammuangsa S., Uttarasak K., Dutchaneephet J., Boonruang C., and Sirikulrat N. (2015) Post-Weld Heat Treatment Effects on Hardness and Impact Strength of Aluminum Alloy 6061 Friction Stir Butt Weld. *Materials Transactions.*

[Woo and Choo, 2011] Woo W. and Choo H. (2011) Softening behavior of friction stir welded Al6061-T6 and Mg AZ31B Alloys.

[Sarabia and Ortiz, 2009] Sarabia L. A. and Ortiz M. C. (2009) Response Surface Methodology.

[Antony, 2014] Antony J. (2014) Full Factorial Design.

[Liu et. al., 2021] Liu Y., Fang D., Zhu B., Wang Y., Li S., and Zhang Y. (2021) Modeling of Isothermal Dissolution of Precipitates in a 6061 Aluminum Allot Sheet During Solution Heat Treatment. *Metals.*

[Chen et. al., 2020] Chen Y., Lu B. Q., and Zhang H. A. (2020) Hardening and Precipitation of a Commercial 6061 Al Alloy During Natural and Artificial Aging. *IOP Conf. Ser.: Mater. Sci. Eng.* 770 012065

[Lee et. al., 2020] Lee H.S., Yoon J.H., and Yoo J. T. (2020) Manufacturing Titanium and Al-Li Alloy Cryogenic Tanks. *Key Engineering Materials Vol. 837*